




Scattering coefficients of superconducting microwave resonators. II. System-bath approach

Qi-Ming Chen ^{1,2,*} Matti Partanen ¹ Florian Fesquet,^{1,2} Kedar E. Honasoge,^{1,2} Fabian Kronowetter,^{1,2} Yuki Nojiri,^{1,2} Michael Renger,^{1,2} Kirill G. Fedorov,^{1,2} Achim Marx ¹ Frank Deppe,^{1,2,3,†} and Rudolf Gross^{1,2,3,‡}

¹Walther-Meißner-Institut, Bayerische Akademie der Wissenschaften, 85748 Garching, Germany

²Physik-Department, Technische Universität München, 85748 Garching, Germany

³Munich Center for Quantum Science and Technology (MCQST), Schellingstr. 4, 80799 Munich, Germany



(Received 22 February 2022; revised 22 November 2022; accepted 28 November 2022; published 9 December 2022)

We describe a unified quantum approach for analyzing the scattering coefficients of superconducting microwave resonators with a variety of geometries, and demonstrate its consistency with the classical approach [Q.-M. Chen *et al.*, *Phys. Rev. B* **106**, 214505 (2022)]. We also generalize the result to a chain of resonators with time delays, and reveal several transport properties similar to a photonic crystal and can be used to design high-quality resonators. These results form a firm theoretical ground for analyzing the scattering coefficients of an arbitrary resonator network. They set a step forward to designing and characterizing superconducting microwave resonators in a complex superconducting quantum circuit.

DOI: [10.1103/PhysRevB.106.214506](https://doi.org/10.1103/PhysRevB.106.214506)

I. INTRODUCTION

Understanding the scattering coefficients of superconducting microwave resonators is crucial to the study of superconducting quantum circuits [1]. Owing to the flexible geometry and the strong interaction in the system, a variety of novel photon transport properties emerge when coupling a microwave resonator to other circuit components [2–19]. For example, it is shown that a dissipative atom can completely reflect the photons propagating along a one-dimensional (1D) waveguide with no loss [2–4], although the physical size of the atom is much smaller than the wavelength of the propagating microwave field. Moreover, microwave resonators can also be coupled to each other with different geometries, which lead to many interesting phenomena such as Fano resonance [20–24], slow light [25–29], coupled-resonator-induced transparency [30–33], and bound states [34–40]. During the past decades, the scattering coefficients of superconducting quantum circuits have attracted an enormous interest and led to a variety of discoveries. However, most of the existing work either assumes the input field to be a few-photon Fock state [41] or considers a purely classical microwave field as the input [42]. Moreover, the existing results are often limited to certain scenarios, although the fundamental concepts behind them, for example, network analysis or input-output analysis, should have a general applicability. For example, one often uses the transfer matrix method to study a hanger-type resonator, but has to switch to the system-bath description when studying a necklace-type resonator [43,44]. A unified approach that applies to a general superconducting microwave resonator is rarely studied, but it is in high demand for designing larger circuits beyond the toy model. Import milestones in theory

include the SLH formalism [45–50], which assumes a unidirectional wave propagation, and the coupled-mode formalism [51–53], which was initially proposed for classical systems.

Here, and also in a parallel paper [54], we study the scattering coefficients of superconducting microwave resonators in either quantum or classical perspectives. In this work, we employ the system-bath method in quantum optics and derive analytically the scattering coefficients of a general resonator [55,56]. We compare the results with the classical approach [54], and reveal the correspondence of different concepts in the two languages, such as the damping rates and the quality factors. We also generalize the method to a chain of microwave resonators, which form a photonic-crystal-like system and exhibit interesting transport features that are qualitatively different from a single resonator. These results provide a systematic study of the scattering coefficients of superconducting microwave resonators in the quantum perspective.

The rest of this paper is organized as follows: In Sec. II, we outline the system-bath method and derive the ideal scattering coefficients of different resonators, which are coupled to the external circuitry with different geometries. We also compare the classical and quantum approaches, and discuss briefly how to deal with experimental imperfections in the quantum approach. Next, we generalize our results to a chain of hanger-type resonators with time delay in Sec. III, which are side coupled to a 1D waveguide with time delays. We also study a chain of necklace-type resonators in Sec. IV, which are coupled to each other end by end. Finally, we conclude this study and discuss how the dephasing effect can be incorporated in the formalism in Sec. V. Detailed derivations of the input-output relations and the scattering coefficients for different resonator networks can be found in Appendixes A–D. Throughout this study, we assume that the frequency range of interest is around the resonance frequency of the fundamental mode by default.

*qiming.chen@wmi.badw.de

†frank.deppe@wmi.badw.de

‡rudolf.gross@wmi.badw.de

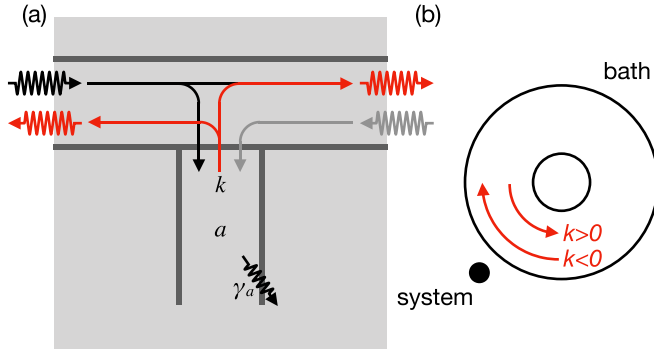


FIG. 1. Schematic of a hanger-type $\lambda/4$ resonator. Here, a short-circuited $\lambda/4$ resonator (i.e., the system) is side coupled to a transmission-line waveguide (i.e., the bath), which accommodates both left- and right-propagating fields. (b) Shows a simplified schematic of (a), where we describe the bath as a circular tube indicating the use of periodic boundary conditions.

II. SCATTERING COEFFICIENTS OF A SINGLE MICROWAVE RESONATOR

A. Hanger-type $\lambda/4$ resonators

The hanger-type $\lambda/4$ resonator is schematically shown in Figs. 1(a) and 1(b), where the intraresonator field a is coupled to the bath field b in the 1D waveguide with a coupling strength κ . We describe the composite system as

$$H_{\text{sys}} = \hbar\omega_r a^\dagger a, \quad (1)$$

$$H_{\text{bth}} = \sum_{k=-\infty}^{+\infty} \hbar\omega_k b_k^\dagger b_k, \quad (2)$$

$$H_{\text{int}} = \sum_{k=-\infty}^{+\infty} \hbar(\kappa^* a b_k^\dagger + \kappa a^\dagger b_k), \quad (3)$$

where ω_r is the resonant frequency, ω_k is the characteristic frequency of the bath field with wave vector k . Following the standard procedure of the input-output analysis [55,56], which is also outlined in Appendix A, one can derive a set of linear equations that relate the dynamics of a to the so-called input and output fields in the bath. However, the input and output fields defined in this way are not directly related to the fields that can be measured in experiments. To calculate the transport properties of the system, one must distinguish the left and the right propagating fields, which we denote as l and r , from the bath b , as shown in Fig. 1(b).

To achieve this goal, we constrain our discussion to a small frequency range around the central driving frequency ω_d . One can approximate the dispersion relation by a linear relation within this small interval [22]

$$\omega_k = \omega_d \mp v_g \Delta_k, \quad (4)$$

where v_g is the group velocity in the waveguide. Besides, $\Delta_k = k \pm k_d$, where k and $k_d > 0$ are the wave vectors that correspond to the frequencies ω_k and ω_d , respectively. In the rotating frame at ω_d , we obtain an equivalent description of the composite system

$$H_{\text{sys}} = \hbar(\omega_r - \omega_d) a^\dagger a, \quad (5)$$

$$H_{\text{bth}} = \sum_{\Delta_k=-\infty}^{+\infty} \hbar v_g \Delta_k (l_{k_r-\Delta_k}^\dagger l_{k_r-\Delta_k} + r_{k_r+\Delta_k}^\dagger r_{k_r+\Delta_k}), \quad (6)$$

$$H_{\text{int}} = \sum_{\Delta_k=-\infty}^{+\infty} \hbar(\kappa^* a l_{k_r-\Delta_k}^\dagger + \kappa^* a r_{k_r+\Delta_k}^\dagger + \text{c.c.}). \quad (7)$$

Here, we have extended the upper and lower limits of the summation to infinity for mathematical convenience, which is valid as long as ω_d is much larger than the typical bandwidth of interest [41]. Finally, we complete our transformation by defining $\omega = v_g \Delta_k$, $\Delta = \omega_r - \omega_d$, and replacing the discrete field operators by a continuum: $l_{k_r-\Delta_k} \rightarrow l_\omega$, $r_{k_r+\Delta_k} \rightarrow r_\omega$. The result is

$$H_{\text{sys}} = \hbar \Delta a^\dagger a, \quad (8)$$

$$H_{\text{bth}} = \int_{-\infty}^{+\infty} d\omega \hbar \omega (l_\omega^\dagger l_\omega + r_\omega^\dagger r_\omega), \quad (9)$$

$$H_{\text{int}} = \int_{-\infty}^{+\infty} d\omega \hbar(\kappa^* a l_\omega^\dagger + \kappa a^\dagger l_\omega + \kappa^* a r_\omega^\dagger + \kappa a^\dagger r_\omega). \quad (10)$$

By separating the left- and right-propagating fields in the waveguide, we split the single physical bath b into two independent baths l and r representing different directions of the propagating fields in a 1D waveguide. We note that this result is consistent with the assumption in Refs. [11,12] for the study of waveguide quantum electrodynamics. In this way, the scattering coefficients of the resonator can be readily obtained by following the standard input-output analysis. Here, we list several major steps for illustration.

Using the Heisenberg equations, we describe the dynamics of a , l_ω , and r_ω as

$$\dot{a} = -i\Delta a - i \int_{-\infty}^{+\infty} d\omega \kappa (l_\omega + r_\omega), \quad (11)$$

$$\dot{l}_\omega = -i\omega l_\omega - i\kappa^* a, \quad (12)$$

$$\dot{r}_\omega = -i\omega r_\omega - i\kappa^* a. \quad (13)$$

We further define the input and output fields corresponding to the two baths as

$$l_{\text{in}} = \frac{1}{\sqrt{2\pi}} \int_{-\infty}^{+\infty} d\omega e^{-i\omega t} l_\omega, \quad l_{\text{out}} = l_{\text{in}} + \sqrt{\gamma} a, \quad (14)$$

$$r_{\text{in}} = \frac{1}{\sqrt{2\pi}} \int_{-\infty}^{+\infty} d\omega e^{-i\omega t} r_\omega, \quad r_{\text{out}} = r_{\text{in}} + \sqrt{\gamma} a, \quad (15)$$

where $\sqrt{\gamma} = i\sqrt{2\pi}\kappa$. Inserting Eqs. (14) and (15) into (11)–(13), we obtain

$$\dot{a} = -i\Delta a - \left(\gamma + \frac{\gamma_a}{2}\right) a - \sqrt{\gamma}(l_{\text{in}} + r_{\text{in}}). \quad (16)$$

Here, we have added the intrinsic damping of the resonator $\gamma_a/2$ by hand. A more rigorous way to include intrinsic damping is to consider an additional bath that is in a thermal state with temperature T and is coupled to a . The result is the same as Eq. (16) for $T \ll \hbar\omega_r/k_B$, where k_B is the Boltzmann constant. We note that this requirement is valid for typical experimental situations in superconducting quantum circuits [57].

Equations (14)–(16) determine the scattering coefficients of a hanger-type $\lambda/4$ resonator, which we formally define as

$$S_{11} = \frac{\langle l_{\text{out}} \rangle}{\langle r_{\text{in}} \rangle}, \quad S_{21} = \frac{\langle r_{\text{out}} \rangle}{\langle r_{\text{in}} \rangle} \text{ with } \langle l_{\text{in}} \rangle = 0; \quad (17)$$

$$S_{12} = \frac{\langle l_{\text{out}} \rangle}{\langle l_{\text{in}} \rangle}, \quad S_{22} = \frac{\langle r_{\text{out}} \rangle}{\langle l_{\text{in}} \rangle} \text{ with } \langle r_{\text{in}} \rangle = 0. \quad (18)$$

That is,

$$S_{11} = S_{22} = -\frac{\gamma}{i\Delta + \left(\gamma + \frac{\gamma_a}{2}\right)}, \quad (19)$$

$$S_{21} = S_{12} = 1 - \frac{\gamma}{i\Delta + \left(\gamma + \frac{\gamma_a}{2}\right)}. \quad (20)$$

We recall that the scattering coefficients of a hanger-type $\lambda/4$ resonator derived in the transfer matrix approach are written as [54]

$$S_{11} = S_{22} \approx -\frac{\frac{\omega_r}{2Q_c}}{i\Delta + \left(\frac{\omega_r}{2Q_i} + \frac{\omega_r}{2Q_c}\right)}, \quad (21)$$

$$S_{21} = S_{12} \approx 1 - \frac{\frac{\omega_r}{2Q_c}}{i\Delta + \left(\frac{\omega_r}{2Q_i} + \frac{\omega_r}{2Q_c}\right)}. \quad (22)$$

Here, we have replaced the imaginary unit j that follows the convention of microwave engineering by the imaginary unit $i = -j$ [58]. We note also that $\Delta = \omega_r - \omega_d$, as defined before. Comparing Eqs. (19) and (20) with (21) and (22), we obtain the following relations between the damping rates and the quality factors:

$$\gamma_a = \frac{\omega_r}{Q_i}, \quad \gamma = \frac{\omega_r}{2Q_c}. \quad (23)$$

The above relations also hold for a hanger-type $\lambda/2$ resonator, but with different definitions of the resonant frequency and the quality factors. We note that the factor of 2 in the expression of γ originates from the fact that both the left- and right-propagating fields in the waveguide are coupled to the intraresonator field. However, the effective energy decay rates in both the internal and coupling dissipation channels are equal to the ratio between the resonant frequency and the corresponding Q factors.

B. Necklace-type $\lambda/2$ resonator

The necklace-type $\lambda/2$ resonator is schematically shown in Figs. 2(a) and 2(b), where the intraresonator field a is coupled to two spatially separated baths b_1 and b_2 on the left- and right-hand sides, respectively. We describe the whole system as

$$H_{\text{sys}} = \hbar\omega_r a^\dagger a, \quad (24)$$

$$H_{\text{bth}} = \sum_{m=1}^2 \sum_{k=0}^{+\infty} \hbar\omega_k b_{m,k}^\dagger b_{m,k}, \quad (25)$$

$$H_{\text{int}} = \sum_{m=1}^2 (-1)^{m-1} \sum_{k=0}^{+\infty} \hbar(\kappa_m^* a b_{m,k}^\dagger + \kappa_m a^\dagger b_{m,k}). \quad (26)$$

Here, the wave vector k takes only positive values that define a unidirectional propagation of the microwave fields in either of the two feedlines, as shown in Fig. 2(b). The phase factor ± 1 in the system-bath interaction takes into account

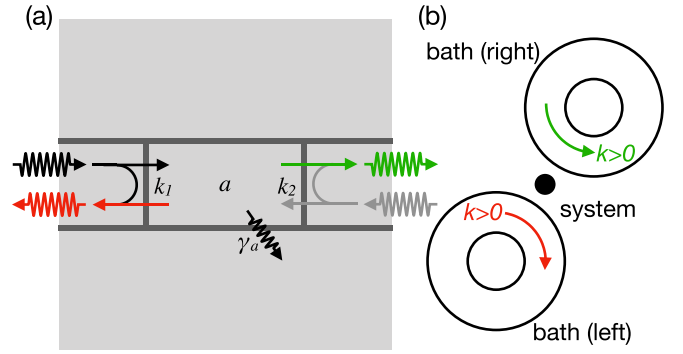


FIG. 2. Schematic of a necklace-type $\lambda/2$ resonator. Here, an open-circuited $\lambda/2$ resonator (i.e., the system) is directly coupled to two transmission-line waveguides (i.e., the baths) at the two ends, respectively. Each of the baths accommodates only one unidirectional propagating field. We use different colors for the two baths to emphasize that they are coupled to the opposite voltage antinodes of the system.

the opposite voltage at the two ends of the resonator for the fundamental normal mode. This convention of sign holds for any *odd* modes, whereas there is no phase difference for the *even* modes.

Following a similar procedure as before, we linearize the dispersion relation around the central driving frequency

$$\omega_k = \omega_d + v_g \Delta k. \quad (27)$$

Eventually, we obtain the Hamiltonian in terms of photon frequencies

$$H_{\text{sys}} = \hbar\Delta a^\dagger a, \quad (28)$$

$$H_{\text{bth}} = \sum_{m=1}^2 \int_{-\infty}^{+\infty} d\omega \hbar\omega b_{m,\omega}^\dagger b_{m,\omega}, \quad (29)$$

$$H_{\text{int}} = \sum_{m=1}^2 (-1)^{m-1} \int_{-\infty}^{+\infty} d\omega \hbar(\kappa_m^* a b_{m,\omega}^\dagger + \kappa_m a^\dagger b_{m,\omega}). \quad (30)$$

Following the Heisenberg equations, we describe the dynamics of a , $b_{1,\omega}$, and $b_{2,\omega}$ as

$$\dot{a} = -i\Delta a - i \sum_{m=1}^2 (-1)^{m-1} \int_{-\infty}^{+\infty} d\omega \kappa_m b_{m,\omega}, \quad (31)$$

$$\dot{b}_{m,\omega} = -i\omega b_{m,\omega} + i(-1)^m \kappa_m^* a, \quad (32)$$

where $m = 1, 2$. We further define the input and output fields corresponding to the two baths as

$$b_{m,\text{in}} = \frac{1}{\sqrt{2\pi}} \int_{-\infty}^{+\infty} d\omega e^{+i\omega t} b_{m,\omega}, \quad (33)$$

$$b_{m,\text{out}} = b_{m,\text{in}} - (-1)^m \sqrt{\gamma_m} a. \quad (34)$$

Inserting Eqs. (33) and (34) into (31) and (32), we obtain

$$\dot{a} = -i\Delta a - \left(\frac{\gamma_1 + \gamma_2}{2} + \frac{\gamma_a}{2}\right) a + \sum_{m=1}^2 (-1)^m \sqrt{\gamma_m} b_{m,\text{in}}. \quad (35)$$

Here, we have defined $\sqrt{\gamma_m} = i\sqrt{2\pi}\kappa_m$ as before and added the intrinsic damping of the resonator $\gamma_a/2$ by hand.

Equations (33)–(35) determine the scattering coefficients of a necklace-type $\lambda/2$ resonator, which we formally define as

$$S_{11} = \frac{\langle b_{1,\text{out}} \rangle}{\langle b_{1,\text{in}} \rangle}, \quad S_{21} = \frac{\langle b_{2,\text{out}} \rangle}{\langle b_{1,\text{in}} \rangle} \text{ with } \langle b_{2,\text{in}} \rangle = 0, \quad (36)$$

$$S_{12} = \frac{\langle b_{1,\text{out}} \rangle}{\langle b_{2,\text{in}} \rangle}, \quad S_{22} = \frac{\langle b_{2,\text{out}} \rangle}{\langle b_{2,\text{in}} \rangle} \text{ with } \langle b_{1,\text{in}} \rangle = 0. \quad (37)$$

That is,

$$S_{11} = 1 - \frac{\gamma_1}{i\Delta + \left(\frac{\gamma_1 + \gamma_2}{2} + \frac{\gamma_a}{2}\right)}, \quad (38)$$

$$S_{21} = S_{12} = \frac{\sqrt{\gamma_1\gamma_2}}{i\Delta + \left(\frac{\gamma_1 + \gamma_2}{2} + \frac{\gamma_a}{2}\right)}, \quad (39)$$

$$S_{22} = 1 - \frac{\gamma_2}{i\Delta + \left(\frac{\gamma_1 + \gamma_2}{2} + \frac{\gamma_a}{2}\right)}. \quad (40)$$

We recall that the scattering coefficients of a necklace-type $\lambda/2$ resonator derived in the transfer matrix approach are written as [54]

$$S_{11} \approx 1 - \frac{\frac{\omega_r}{Q_{e,1}}}{i\Delta + \left(\frac{\omega_r}{2Q_i} + \frac{\omega_r}{2Q_{e,1}} + \frac{\omega_r}{2Q_{e,2}}\right)}, \quad (41)$$

$$S_{21} = S_{12} \approx \frac{\frac{\omega_r}{\sqrt{Q_{e,1}Q_{e,2}}}}{i\Delta + \left(\frac{\omega_r}{2Q_i} + \frac{\omega_r}{2Q_{e,1}} + \frac{\omega_r}{2Q_{e,2}}\right)}, \quad (42)$$

$$S_{22} \approx 1 - \frac{\frac{\omega_r}{Q_{e,2}}}{i\Delta + \left(\frac{\omega_r}{2Q_i} + \frac{\omega_r}{2Q_{e,1}} + \frac{\omega_r}{2Q_{e,2}}\right)}. \quad (43)$$

Comparing Eqs. (38)–(40) with (41)–(43), we obtain the following relations between the damping rates and the quality factors:

$$\gamma_a = \frac{\omega_r}{Q_i}, \quad \gamma_1 = \frac{\omega_r}{Q_{e,1}}, \quad \gamma_2 = \frac{\omega_r}{Q_{e,2}}. \quad (44)$$

These relations also hold for a necklace-type $\lambda/4$ resonator but with different definitions of the resonant frequency and the quality factors.

C. Cross-type $\lambda/2$ resonators

The cross-type $\lambda/2$ resonator is schematically shown in Figs. 3(a) and 3(b), where the intraresonator field a is coupled to two spatially separated baths b_1 and b_2 on the left and right sides, respectively. Here, we assume that the two feedlines are coupled to the same voltage antinode of the bare resonator. Compared with the necklace-type $\lambda/2$ resonator, the major difference of the composite Hamiltonian lies in the system-bath interaction

$$H_{\text{int}} = \sum_{m=1}^2 \sum_{k=0}^{+\infty} \hbar(\kappa_m^* a b_{m,k}^\dagger + \kappa_m a^\dagger b_{m,k}). \quad (45)$$

Consequently, the input-output relations are similar as before:

$$\dot{a} = -i\Delta a - \left(\frac{\gamma_1 + \gamma_2}{2} + \frac{\gamma_a}{2}\right)a - \sum_{m=1}^2 \sqrt{\gamma_m} b_{m,\text{in}}, \quad (46)$$

$$b_{m,\text{out}} = b_{m,\text{in}} + \sqrt{\gamma_m} a, \quad (47)$$

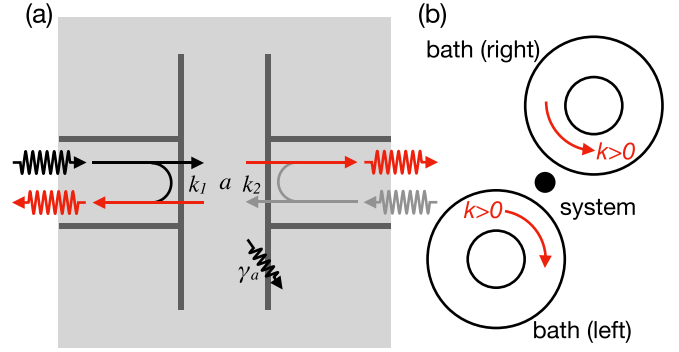


FIG. 3. Schematic of a cross-type $\lambda/2$ resonator. Here, a short-circuited $\lambda/2$ resonator (i.e., the system) is directly coupled to two transmission-line waveguides (i.e., the baths) at the same voltage antinode. Each of the baths accommodates only one unidirectional propagating field.

where $m = 1, 2$. Here, we have also added the intrinsic damping $\gamma_a/2$ by hand. The scattering coefficients of a cross-type $\lambda/2$ resonator are

$$S_{11} = 1 - \frac{\gamma_1}{i\Delta + \left(\frac{\gamma_1 + \gamma_2}{2} + \frac{\gamma_a}{2}\right)}, \quad (48)$$

$$S_{21} = S_{12} = -\frac{\sqrt{\gamma_1\gamma_2}}{i\Delta + \left(\frac{\gamma_1 + \gamma_2}{2} + \frac{\gamma_a}{2}\right)}, \quad (49)$$

$$S_{22} = 1 - \frac{\gamma_2}{i\Delta + \left(\frac{\gamma_1 + \gamma_2}{2} + \frac{\gamma_a}{2}\right)}. \quad (50)$$

We recall that the scattering coefficients of a cross-type $\lambda/2$ resonator, which have been derived by using the classical transfer matrix approach [54], as

$$S_{11} \approx 1 - \frac{\frac{\omega_r}{Q_{e,1}}}{i\Delta + \left(\frac{\omega_r}{2Q_i} + \frac{\omega_r}{2Q_{e,1}} + \frac{\omega_r}{2Q_{e,2}}\right)}, \quad (51)$$

$$S_{21} = S_{12} \approx \frac{\frac{\omega_r}{\sqrt{Q_{e,1}Q_{e,2}}}}{i\Delta + \left(\frac{\omega_r}{2Q_i} + \frac{\omega_r}{2Q_{e,1}} + \frac{\omega_r}{2Q_{e,2}}\right)}, \quad (52)$$

$$S_{22} \approx 1 - \frac{\frac{\omega_r}{Q_{e,2}}}{i\Delta + \left(\frac{\omega_r}{2Q_i} + \frac{\omega_r}{2Q_{e,1}} + \frac{\omega_r}{2Q_{e,2}}\right)}. \quad (53)$$

Comparing Eqs. (48)–(50) with (51)–(53), we obtain the following relations between the decay rates and the quality factors:

$$\gamma_a = \frac{\omega_r}{Q_i}, \quad \gamma_1 = \frac{\omega_r}{Q_{e,1}}, \quad \gamma_2 = \frac{\omega_r}{Q_{e,2}}. \quad (54)$$

D. Comparison with the transfer matrix approach

So far, we have considered the scattering coefficients of a general and ideal superconducting microwave resonator. Generally speaking, a superconducting microwave resonator is a two-port system. The key procedure to perform input-output analysis is to describe the fields measured at the two ports by two separate baths. This separation is natural for necklace- and cross-type resonators, where the baths are already separated in space [43,44]. However, analyzing the input-output relation of a hanger-type resonator is not a trivial task because the bare resonator is coupled to one single bath in space. Here, we start the analysis from the wave-vector space. We linearize

the dispersion relation of the waveguide around the frequency of interest [22], and transform the Hamiltonian from the wave-vector space to the frequency space with two separated baths. Effectively, we artificially separate the single physical bath into two independent baths with opposite propagation directions, and perform input-output analysis thereafter. Once we obtain the input-output relation, the scattering coefficients can be readily calculated by taking the mean value of the field operators. Depending on the specific geometry of the system, one may use Eqs. (17) and (18) for hanger-type resonators, or in Eqs. (36) and (37) for necklace- or cross-type resonators.

Compared with the tedious calculations in the transfer matrix approach [54], the system-bath approach provides a shortcut to the same analytical result. This advantage originates from a high-level abstraction of the system, which describes a circuit with only a few parameters and assumes the validity of the Born and Markov approximations [59]. However, this convenience comes with the drawback that it does not relate the results directly to the circuit parameters. Although this is not an issue for characterization purposes, it causes convenience for the circuit design. Given a bunch of circuit parameters, one needs to follow the transfer matrix approach to calculate the abstract parameters, such as the resonant frequency and coupling strength, before using the system-bath approach. If we consider further the experimental imperfections in the system, the system-bath approach can be rather complicated. For example, to take circuit asymmetry into consideration one may consider coupling the composite system to an even larger bath which accommodates both the ideal input and output fields and the impedance-mismatch-induced reflection fields. In these regards, a combination of the transfer matrix and the system-bath approaches may be a more practical choice for describing a practical resonator or a resonator network introduced shortly. Here, the former is useful for abstracting the circuit parameters and capturing the circuit imperfections, while the latter is convenient for analyzing the ideal scattering responses of the system.

III. COUPLING MULTIPLE HANGER-TYPE RESONATORS TO A LONG WAVEGUIDE

A. General scattering coefficients

Let us now consider a more complex system with N hanger-type resonators, denoted by a_j , that are side coupled

to a 1D waveguide, as schematically shown in Figs. 4(a) and 4(b). Following the discussions in Sec. II C, we separate the left- and right-propagating fields in the waveguide and describe them as two independent baths. The total Hamiltonian is

$$H_{\text{sys}} = \sum_{j=1}^N \hbar \Delta_j a_j^\dagger(t) a_j(t), \quad (55)$$

$$H_{\text{bth}} = \int_{-\infty}^{+\infty} d\omega \hbar \omega [l_\omega^\dagger(t) l_\omega(t) + r_\omega^\dagger(t) r_\omega(t)], \quad (56)$$

$$H_{\text{int}} = \sum_{j=1}^N \int_{-\infty}^{+\infty} d\omega \hbar \{ \kappa_j^* a_j(t) l_\omega^\dagger[t + (j-1)\tau] + \kappa_j^* a_j(t) r_\omega^\dagger[t - (j-1)\tau] + \text{c.c.} \}. \quad (57)$$

Here, we explicitly included the time delay in the system-bath interaction because the resonators are coupled to the waveguide at different positions. The \pm sign of the delay in l_ω and r_ω originates from their opposite propagating directions in the waveguide. Following the derivations in Appendix B, we obtain the following relation that describes the dynamics of the j th intraresonator field:

$$\dot{a}_j = -i\Delta_j a_j - \frac{\gamma_{a,j}}{2} a_j - \sum_{j'=1}^N \sqrt{\gamma_{j'}} (\sqrt{\gamma_{j'}})^* e^{i(j'-j)\theta} a_{j'}(t) - \sqrt{\gamma_{j'}} l_{\text{in}}(t) e^{-i(j-N)\theta} - \sqrt{\gamma_{j'}} r_{\text{in}}(t) e^{i(j-1)\theta}. \quad (58)$$

Here, $\theta = \omega_d \tau$ with ω_d being the central driving frequency and τ the time delay of the propagating field traveling between two adjacent resonators. The operators l_{in} and r_{in} are, respectively, defined as the input fields at the right- and left-hand sides of the waveguide, which propagate in opposite directions, as shown in Fig. 4(b). Correspondingly, we respectively define l_{out} and r_{out} as the output fields at the left- and right-hand sides of the waveguide

$$l_{\text{out}} = e^{i(N-1)\theta} l_{\text{in}} + \sum_{j'=1}^N (\sqrt{\gamma_{j'}})^* e^{i(j'-1)\theta} a_{j'}, \quad (59)$$

$$r_{\text{out}} = e^{i(N-1)\theta} r_{\text{in}} + \sum_{j'=1}^N (\sqrt{\gamma_{j'}})^* e^{i(N-j')\theta} a_{j'}. \quad (60)$$

With these definitions, the scattering coefficients of the resonator chain can be readily obtained by using the expression in Eqs. (17) and (18). For example, for the simplest case with $N = 2$ we have

$$S_{11} = -\frac{\gamma_1(i\Delta_2 + \gamma_{a,2}) + e^{i2\theta} \gamma_2(i\Delta_1 + \gamma_{a,1}) + \gamma_1 \gamma_2 (1 - e^{i2\theta})}{(i\Delta_1 + \gamma_{a,1})(i\Delta_2 + \gamma_{a,2}) + \gamma_1(i\Delta_2 + \gamma_{a,2}) + \gamma_2(i\Delta_1 + \gamma_{a,1}) + \gamma_1 \gamma_2 (1 - e^{i2\theta})}, \quad (61)$$

$$S_{21} = S_{12} = \frac{e^{i\theta} (i\Delta_1 + \gamma_{a,1})(i\Delta_2 + \gamma_{a,2})}{(i\Delta_1 + \gamma_{a,1})(i\Delta_2 + \gamma_{a,2}) + \gamma_1(i\Delta_2 + \gamma_{a,2}) + \gamma_2(i\Delta_1 + \gamma_{a,1}) + \gamma_1 \gamma_2 (1 - e^{i2\theta})}, \quad (62)$$

$$S_{22} = -\frac{e^{i2\theta} \gamma_1(i\Delta_2 + \gamma_{a,2}) + \gamma_2(i\Delta_1 + \gamma_{a,1}) + \gamma_1 \gamma_2 (1 - e^{i2\theta})}{(i\Delta_1 + \gamma_{a,1})(i\Delta_2 + \gamma_{a,2}) + \gamma_1(i\Delta_2 + \gamma_{a,2}) + \gamma_2(i\Delta_1 + \gamma_{a,1}) + \gamma_1 \gamma_2 (1 - e^{i2\theta})}. \quad (63)$$

This result is equivalent to that reported in Refs. [20,23], but with different methods in the derivation.

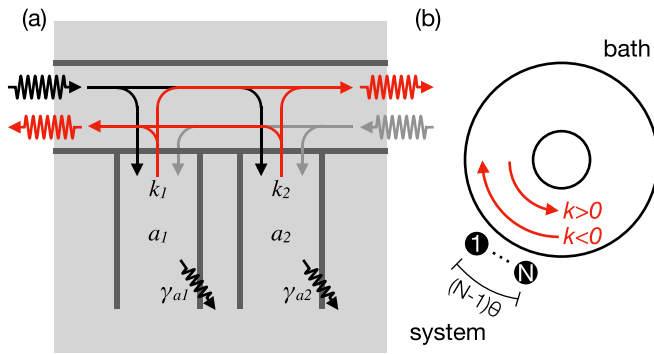


FIG. 4. Schematic of a chain of N hanger-type $\lambda/4$ resonators (i.e., the system) that are side coupled to a 1D transmission-line waveguide (i.e., the bath). The bath accommodates both left- and right-propagating fields. We denote the time delay between a propagating photon and two adjacent resonators as a phase factor θ .

B. Simulation results

For large N , it is rather cumbersome to derive an analytical expression for the scattering coefficients. Fortunately, efficient numerical algorithms exist if we simplify the discussion to $\Delta_j \equiv \Delta$ and $\gamma_{a,j} \equiv \gamma_a$, as discussed in Appendix C. Here, we perform several numerical simulations to cross-check the analytical results derived above. The numerical simulation is performed by multiplying the transfer matrices of different circuit components at different frequencies. The parameters are chosen as follows: real propagating constant $\alpha = 5.0 \times 10^{-3} \text{ m}^{-1}$, phase velocity $v_{\text{ph}} = 1.35 \times 10^8 \text{ m/s}$, characteristic impedance $Z_0 = 50 \text{ } \Omega$, coupling capacitor $C = 1.0 \times 10^{-14} \text{ F}$. The length of each hanger-type $\lambda/4$ resonator is $l = 5.0 \times 10^{-3} \text{ m}$. Following the transfer matrix approach, we find the resonant frequency of each individual resonator as $\omega_r = 2\pi \times 6.659 \text{ GHz}$, and also the coupling and internal decay rates $\gamma = 5.83 \text{ MHz}$ and $\gamma_a = 1.33 \text{ MHz}$ [54].

In Fig. 5(a), we vary the phase difference θ , i.e., the distance between neighboring resonators, and calculate the scattering coefficients for $N = 2$. On the one hand, the absolute value of the reflection and transmission amplitudes exhibits an asymmetric Fano resonance line shape for $\theta \neq n\pi/2$ with $n = 0, 1, \dots$ [23]. Depending on whether $\theta = n\pi$ or $n\pi + \pi/2$, we obtain a symmetric Lorentzian spectrum, also known as the Breit-Wigner resonance [60], or a symmetric Fano spectrum [61], respectively. These line shapes can be better seen in Fig. 5(d), where we fix θ to several values. On the other hand, a transition between the symmetric and asymmetric line spectra occurs at $\theta = n\pi/2$. As can be seen in the corresponding phase diagrams, the transition is smooth at $\theta = n\pi$. However, an abrupt π -phase shift happens for every $\theta = n\pi + \pi/2$, which distinguishes the symmetric Lorentzian spectrum from the symmetric Fano spectrum. With the increase of N , the transition between the symmetric and asymmetric line shapes occurs more frequently at $\theta = n\pi + 2n'\pi/2^N$ for $n = 0, 1, \dots$ and $n' = 1, \dots, n-1$, as shown in Figs. 5(a)–5(c). Correspondingly, the sudden π -phase change happens at $\theta = (2n+1)\pi/2^N$.

We also compare the reflection line shape for different N and θ in Fig. 5(d). It can be clearly seen that the phase factor θ determines whether a broadening or narrowing of the spectrum is to be observed with an increasing N . For example, the full width at half-maximum (FWHM) increases monotonically with N for $\theta = 0$, or equivalently 2π , while it decreases monotonically for $\theta = \pi/2$. These observations indicate that, by coupling multiple hanger-type resonators alongside a waveguide, one can engineer the scattering coefficients of the composite system and obtain an effective microwave resonator. Depending on the parameter θ , this photonic-crystal-like resonator can have a huge enhancement or reduction of the Q factors compared with each individual hanger-type resonator, which provides a new freedom to the design of superconducting microwave resonators.

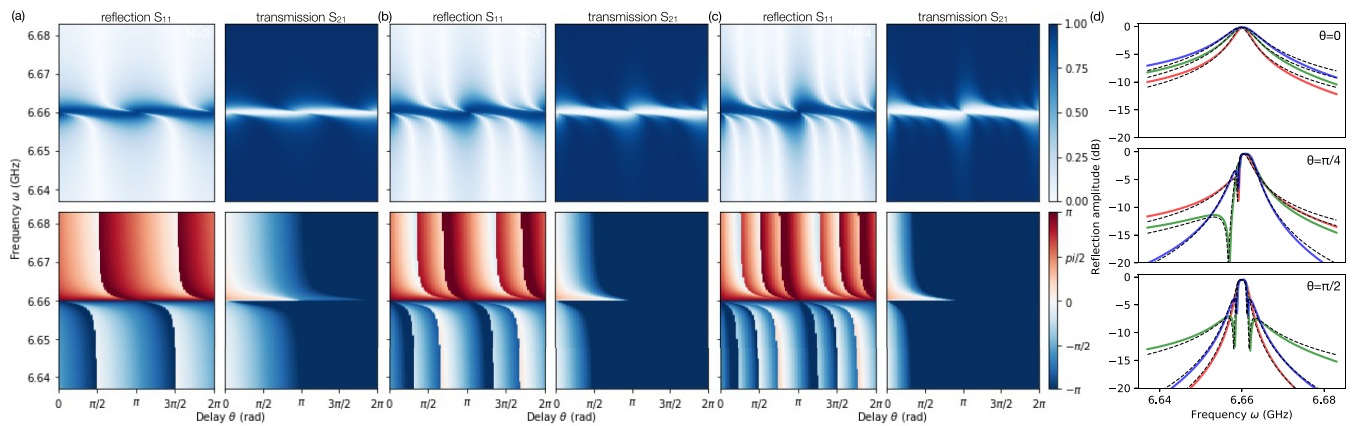


FIG. 5. Scattering coefficients of a chain of N hanger-type $\lambda/4$ resonators, which are side coupled to a 1D waveguide. (a) For $N = 2$, the spectrum periodically changes from a symmetric to an asymmetric line shape with θ . The symmetric line shapes are obtained at $\theta = n\pi/2$, while there exists a sudden π -phase change for every $\theta = n\pi + \pi/2$. (b), (c) With the increase of N , the change of line shape happens more frequently with a varying θ . Here, sudden π -phase changes occur at $\theta = (2n+1)\pi/2^N$ for $n = 1, \dots, N-1$. (d) The reflection responses for $\theta = 0, \pi/4, \pi/2$ (top, middle, bottom) and $N = 2, 3, 4$ (red, green, blue). The black dashed curves indicate the results derived in the system-bath approach, while the solid ones by using ABCD matrices. The resonant frequency ω_r is calculated by using the method introduced in Ref. [54], which is shifted by 1 MHz for a better fitting.

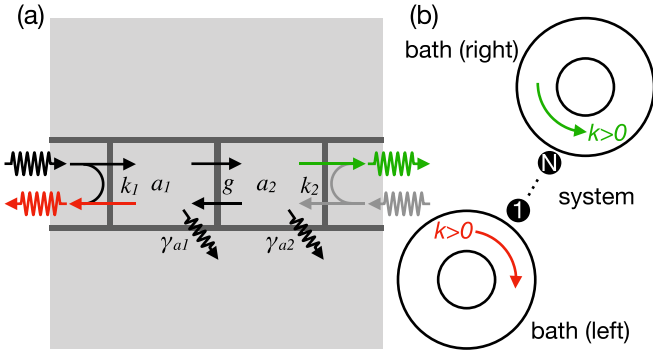


FIG. 6. Schematic of a chain of coupled necklace-type $\lambda/2$ resonators (i.e., the system), which is coupled to two transmission-line waveguides (i.e., the baths) at the two ends, respectively. Each of the baths accommodates only one unidirectional propagating field. We use different colors for the two baths to emphasize that they are coupled to the opposite voltage antinodes of the system.

IV. COUPLING MULTIPLE NECKLACE-TYPE RESONATORS IN A CHAIN

A. General scattering coefficients

Aside from coupling multiple hanger-type resonators to a 1D waveguide, one may also consider coupling N necklace-

$$\dot{a}_j = \begin{cases} -i\Delta_1 a_1 + ig_1 a_2 - \left(\frac{\gamma_1}{2} + \frac{\gamma_{a,1}}{2}\right) a_1 - \sqrt{\gamma_1} b_{1,\text{in}} & \text{for } j = 1; \\ -i\Delta_j a_j + i(g_{j-1} a_{j-1} + g_j a_{j+1}) - \frac{\gamma_{a,j}}{2} a_j & \text{for } 1 < j < N; \\ -i\Delta_N a_N + ig_{N-1} a_{N-1} - \left(\frac{\gamma_2}{2} + \frac{\gamma_{a,N}}{2}\right) a_N + \sqrt{\gamma_2} b_{2,\text{in}} & \text{for } j = N. \end{cases} \quad (69)$$

Similar to the single-resonator case, the scattering coefficients can be obtained by calculating the mean-field steady-state solution of Eqs. (67)–(69). For example, for the simplest case with $N = 2$, we have

$$S_{11} = 1 - \frac{\gamma_1 [i\Delta_2 + (\frac{\gamma_2}{2} + \frac{\gamma_{a,2}}{2})]}{[i\Delta_1 + (\frac{\gamma_1}{2} + \frac{\gamma_{a,1}}{2})][i\Delta_2 + (\frac{\gamma_2}{2} + \frac{\gamma_{a,2}}{2})] + g_1^2}, \quad (70)$$

$$S_{21} = S_{12} = \frac{-ig_1 \sqrt{\gamma_1 \gamma_2}}{[i\Delta_1 + (\frac{\gamma_1}{2} + \frac{\gamma_{a,1}}{2})][i\Delta_2 + (\frac{\gamma_2}{2} + \frac{\gamma_{a,2}}{2})] + g_1^2}, \quad (71)$$

$$S_{22} = 1 - \frac{\gamma_2 [i\Delta_1 + (\frac{\gamma_1}{2} + \frac{\gamma_{a,1}}{2})]}{[i\Delta_1 + (\frac{\gamma_1}{2} + \frac{\gamma_{a,1}}{2})][i\Delta_2 + (\frac{\gamma_2}{2} + \frac{\gamma_{a,2}}{2})] + g_1^2}. \quad (72)$$

This result has been derived and experimentally demonstrated in our previous work [62].

B. Tight-binding model

To get physical insight beyond the numerical solutions for large N , we assume that $\Delta_j \equiv \Delta$, $g_j \equiv g$, and $\gamma_{a,j} \equiv \gamma_a$. In this way, the resonator chain can be described as a bosonic tight-binding model. For a finite number of resonators N , we

type resonators with each other and form a 1D chain of resonators, as schematically shown in Figs. 6(a) and 6(b). The total Hamiltonian reads as

$$H_{\text{sys}} = \sum_{j=1}^N \hbar \Delta_j a_j^\dagger a_j - \hbar g_j (a_j^\dagger a_{j+1} + a_j a_{j+1}^\dagger), \quad (64)$$

$$H_{\text{bth}} = \sum_{m=1}^2 \int_{-\infty}^{+\infty} d\omega \hbar \omega b_{m,\omega}^\dagger b_{m,\omega}, \quad (65)$$

$$H_{\text{int}} = \int_{-\infty}^{+\infty} d\omega \hbar (\kappa_1^* a_1 b_{1,\omega}^\dagger - \kappa_2^* a_N b_{2,\omega}^\dagger + \text{c.c.}), \quad (66)$$

where g_j is the coupling strength between the j th and $(j+1)$ th resonators. The input-output relations can be readily obtained by following the standard procedure

$$b_{1,\text{out}} = b_{1,\text{in}} + \sqrt{\gamma_1} a_1, \quad (67)$$

$$b_{2,\text{out}} = b_{2,\text{in}} - \sqrt{\gamma_2} a_N, \quad (68)$$

while the dynamics of the j th intracavity field reads as

define the following collective modes of the system:

$$c_k = \sum_{j=1}^N \sqrt{\frac{2}{N+1}} \sin\left(\frac{\pi k j}{N+1}\right) a_j. \quad (73)$$

This replacement of variable is similar to the definition of magnon in spin systems [63]. It allows us to rewrite Eqs. (67)–(69) in a more compact form:

$$b_{1,\text{out}} = b_{1,\text{in}} + \sum_{k=1}^N \sqrt{\gamma_{1,k}} c_k, \quad (74)$$

$$b_{2,\text{out}} = b_{2,\text{in}} + \sum_{k=1}^N (-1)^k \sqrt{\gamma_{2,k}} c_k, \quad (75)$$

$$\begin{aligned} \dot{c}_k = & - \left(i\Delta_k + \frac{\gamma_a}{2} \right) c_k - [\sqrt{\gamma_{1,k}} b_{1,\text{in}} + (-1)^k \sqrt{\gamma_{2,k}} b_{2,\text{in}}] \\ & - \frac{1}{2} \sum_{k'=1}^N [\sqrt{\gamma_{1,k} \gamma_{1,k'}} + (-1)^{k+k'} \sqrt{\gamma_{2,k} \gamma_{2,k'}}] c_{k'}. \end{aligned} \quad (76)$$

Here, $\Delta_k = \Delta - 2g \cos[k\pi(N+1)]$ and $\sqrt{\gamma_{m,k}} = \sqrt{2\gamma_m/(N+1)} \sin[k\pi/(N+1)]$. With these input-output relations, one can readily obtain the following analytical expressions for the scattering coefficients (see Appendix D

for detail):

$$S_{11} = 1 - \frac{\left(1 + \frac{1}{2} \sum_{k=1}^N \frac{\gamma_{2,k}}{i\Delta_k + \frac{\gamma_a}{2}}\right) \left(\sum_{k=1}^N \frac{\gamma_{1,k}}{i\Delta_k + \frac{\gamma_a}{2}}\right) - \frac{1}{2} \left(\sum_{k=1}^N \frac{(-1)^k \sqrt{\gamma_{1,k}\gamma_{2,k}}}{i\Delta_k + \frac{\gamma_a}{2}}\right)^2}{\left(1 + \frac{1}{2} \sum_{k=1}^N \frac{\gamma_{1,k}}{i\Delta_k + \frac{\gamma_a}{2}}\right) \left(1 + \frac{1}{2} \sum_{k=1}^N \frac{\gamma_{2,k}}{i\Delta_k + \frac{\gamma_a}{2}}\right) - \left(\frac{1}{2} \sum_{k=1}^N \frac{(-1)^k \sqrt{\gamma_{1,k}\gamma_{2,k}}}{i\Delta_k + \frac{\gamma_a}{2}}\right)^2}, \quad (77)$$

$$S_{21} = S_{12} = - \frac{\left(\sum_{k=1}^N \frac{(-1)^k \sqrt{\gamma_{1,k}\gamma_{2,k}}}{i\Delta_k + \frac{\gamma_a}{2}}\right)}{\left(1 + \frac{1}{2} \sum_{k=1}^N \frac{\gamma_{1,k}}{i\Delta_k + \frac{\gamma_a}{2}}\right) \left(1 + \frac{1}{2} \sum_{k=1}^N \frac{\gamma_{2,k}}{i\Delta_k + \frac{\gamma_a}{2}}\right) - \left(\frac{1}{2} \sum_{k=1}^N \frac{(-1)^k \sqrt{\gamma_{1,k}\gamma_{2,k}}}{i\Delta_k + \frac{\gamma_a}{2}}\right)^2}, \quad (78)$$

$$S_{22} = 1 - \frac{\left(1 + \frac{1}{2} \sum_{k=1}^N \frac{\gamma_{1,k}}{i\Delta_k + \frac{\gamma_a}{2}}\right) \left(\sum_{k=1}^N \frac{\gamma_{2,k}}{i\Delta_k + \frac{\gamma_a}{2}}\right) - \frac{1}{2} \left(\sum_{k=1}^N \frac{(-1)^k \sqrt{\gamma_{1,k}\gamma_{2,k}}}{i\Delta_k + \frac{\gamma_a}{2}}\right)^2}{\left(1 + \frac{1}{2} \sum_{k=1}^N \frac{\gamma_{1,k}}{i\Delta_k + \frac{\gamma_a}{2}}\right) \left(1 + \frac{1}{2} \sum_{k=1}^N \frac{\gamma_{2,k}}{i\Delta_k + \frac{\gamma_a}{2}}\right) - \left(\frac{1}{2} \sum_{k=1}^N \frac{(-1)^k \sqrt{\gamma_{1,k}\gamma_{2,k}}}{i\Delta_k + \frac{\gamma_a}{2}}\right)^2}. \quad (79)$$

We note that the definition of collective modes in Eq. (73) is valid for a linear chain with a finite number of microwave resonators. Alternatively, one may also consider an N -resonator loop or an infinitely long chain with $N \rightarrow \infty$. In this situation, the collective modes should be defined in a slightly different way:

$$c_k = \sum_{j=1}^N \sqrt{\frac{1}{N}} \exp\left(\frac{i2\pi k j}{N}\right) a_j. \quad (80)$$

Here, $\Delta_k = \Delta - 2g \cos(2k\pi/N)$, $\sqrt{\gamma_{1,k}} = \sqrt{\gamma_1/N} \exp[-i2\pi k/N]$, and $\sqrt{\gamma_{2,k}} = \sqrt{\gamma_2/N}$. The input-output relations are

$$b_{1,\text{out}} = b_{1,\text{in}} + \sum_{k=1}^N \sqrt{\gamma_{1,k}} c_k, \quad (81)$$

$$b_{2,\text{out}} = b_{2,\text{in}} - \sum_{k=1}^N \sqrt{\gamma_{2,k}} c_k, \quad (82)$$

$$\dot{c}_k = -\left(i\Delta_k + \frac{\gamma_a}{2}\right) c_k - [\sqrt{\gamma_{1,k}} b_{1,\text{in}} - \sqrt{\gamma_{2,k}} b_{2,\text{in}}] - \frac{1}{2} \sum_{k'=1}^N [\sqrt{\gamma_{1,k}\gamma_{1,k'}} + \sqrt{\gamma_{2,k}\gamma_{2,k'}}] c_{k'}, \quad (83)$$

and the scattering coefficients read as

$$S_{11} = 1 - \frac{\left(1 + \frac{1}{2} \sum_{k=1}^N \frac{\gamma_{2,k}}{i\Delta_k + \frac{\gamma_a}{2}}\right) \left(\sum_{k=1}^N \frac{\gamma_{1,k}}{i\Delta_k + \frac{\gamma_a}{2}}\right) - \frac{1}{2} \left(\sum_{k=1}^N \frac{\sqrt{\gamma_{1,k}\gamma_{2,k}}}{i\Delta_k + \frac{\gamma_a}{2}}\right)^2}{\left(1 + \frac{1}{2} \sum_{k=1}^N \frac{\gamma_{1,k}}{i\Delta_k + \frac{\gamma_a}{2}}\right) \left(1 + \frac{1}{2} \sum_{k=1}^N \frac{\gamma_{2,k}}{i\Delta_k + \frac{\gamma_a}{2}}\right) - \left(\frac{1}{2} \sum_{k=1}^N \frac{\sqrt{\gamma_{1,k}\gamma_{2,k}}}{i\Delta_k + \frac{\gamma_a}{2}}\right)^2}, \quad (84)$$

$$S_{21} = S_{12} = \frac{\left(\sum_{k=1}^N \frac{\sqrt{\gamma_{1,k}\gamma_{2,k}}}{i\Delta_k + \frac{\gamma_a}{2}}\right)}{\left(1 + \frac{1}{2} \sum_{k=1}^N \frac{\gamma_{1,k}}{i\Delta_k + \frac{\gamma_a}{2}}\right) \left(1 + \frac{1}{2} \sum_{k=1}^N \frac{\gamma_{2,k}}{i\Delta_k + \frac{\gamma_a}{2}}\right) - \left(\frac{1}{2} \sum_{k=1}^N \frac{\sqrt{\gamma_{1,k}\gamma_{2,k}}}{i\Delta_k + \frac{\gamma_a}{2}}\right)^2}, \quad (85)$$

$$S_{22} = 1 - \frac{\left(1 + \frac{1}{2} \sum_{k=1}^N \frac{\gamma_{1,k}}{i\Delta_k + \frac{\gamma_a}{2}}\right) \left(\sum_{k=1}^N \frac{\gamma_{2,k}}{i\Delta_k + \frac{\gamma_a}{2}}\right) - \frac{1}{2} \left(\sum_{k=1}^N \frac{\sqrt{\gamma_{1,k}\gamma_{2,k}}}{i\Delta_k + \frac{\gamma_a}{2}}\right)^2}{\left(1 + \frac{1}{2} \sum_{k=1}^N \frac{\gamma_{1,k}}{i\Delta_k + \frac{\gamma_a}{2}}\right) \left(1 + \frac{1}{2} \sum_{k=1}^N \frac{\gamma_{2,k}}{i\Delta_k + \frac{\gamma_a}{2}}\right) - \left(\frac{1}{2} \sum_{k=1}^N \frac{\sqrt{\gamma_{1,k}\gamma_{2,k}}}{i\Delta_k + \frac{\gamma_a}{2}}\right)^2}. \quad (86)$$

C. Simulation results

As a cross-check of the analytical results derived above, we performed several numerical simulations with the same parameters as before. Similarly, the numerical simulation is performed by multiplying the transfer matrices of different circuit components at different frequencies. However, the resonator length is extended to $l = 1.0 \times 10^{-2}$ m for $\lambda/2$ resonators. Following the transfer matrix approach, we find the resonant frequency of each individual resonator as $\omega_r = 2\pi \times 6.659$ GHz, and also the coupling and internal decay rates $\gamma = 11.68$ MHz and $\gamma_a = 1.33$ MHz.

In Fig. 7(a), we calculate the scattering coefficients with a varying number of resonators N . The number of peaks (dips) increases with N as expected. However, the spread of the

resonant frequencies also scales with N but saturates to a finite value. The bandwidth is approximately four times of the coupling strength, $g \approx 2\pi \times 44$ MHz, which is calculated by using the method introduced in Ref. [54]. These phenomena can be readily understood in the dispersion relation of the collective fields c_k . A more detailed inspection of the spectrum around ω_r indicates that the photons at the central resonant frequency can be fully transmitted or reflected, depending on the *oddness* and *evenness* of N , as shown in Fig. 7(b). This observation indicates a possible application that a chain of coupled resonators can be used as a single-photon switch [64,65]. Moreover, we observe that the FWHM of the line shape decreases monotonically with N , as shown in Fig. 7(c). It indicates the existence of a high- Q mode in an array of

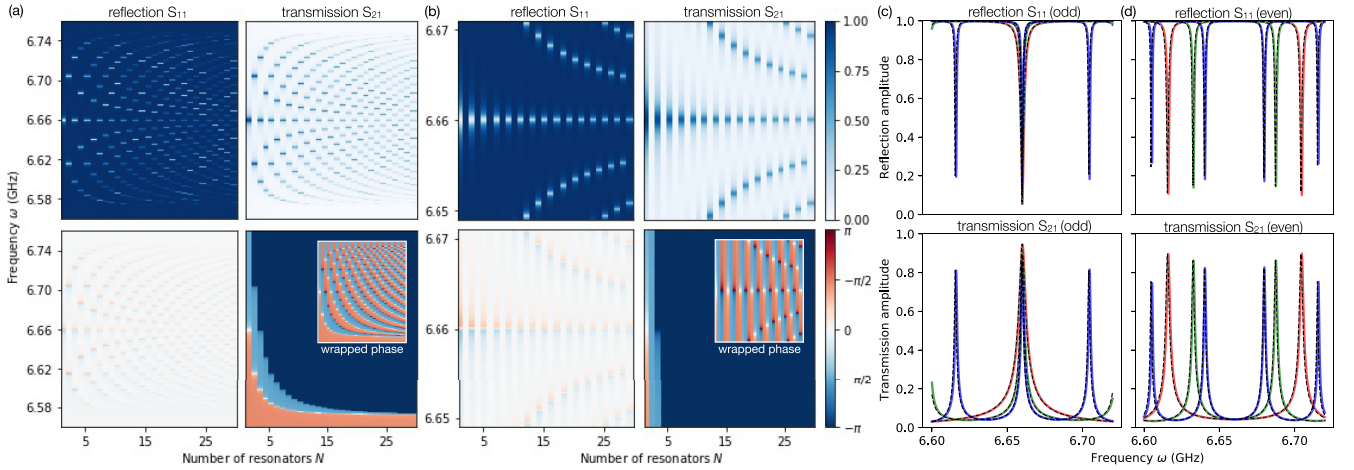


FIG. 7. Scattering coefficients of a chain of coupled necklace-type $\lambda/4$ resonators, which is coupled to two feedlines at the two ends. (a) With the increase of N , there emerges the same number of resonance dips and peaks in the reflection and transmission responses, respectively. The spread of the peaks (dips) saturates at a value which is equal to 4 times of the coupling strength. (b) A closer inspection of the spectrum around the central resonant frequency indicates that the incident photons can be fully reflected or transmitted depending on the parity of N . The FWHM of the central peak also decreases monotonically with N . (c) The reflection and transmission responses for $N = 2, 3, 4$ (red, green, blue), respectively. The black dashed curves indicate the results derived in the system-bath approach, while the solid ones by using ABCD matrices. The resonant frequency ω_r is calculated by using the method introduced in Ref. [54], which is shifted by 1 MHz for a better fitting.

coupled necklace-type resonators. Similar results in optics have been theoretically predicted by using the transfer matrix method and experimentally observed [26,66–68]. Together with the results in Sec. III, we conclude that the interactions between resonators can fundamentally change the scattering coefficients of a bare resonator. It is possible to achieve a high- Q mode by coupling multiple low- Q resonators. The resulting system is called the coupled resonator optical waveguide (CROW) in optics [42], which is one of the prevalent ways for making a high- Q photonic crystal resonator [69,70].

V. CONCLUSIONS AND OUTLOOK

In conclusion, we provide a comprehensive study of the scattering coefficients of superconducting microwave resonators in the quantum perspective. By transforming the Hamiltonian from the wave-vector space to the frequency space, we report a unified approach for input-output analysis that applies to a general microwave resonator. The corresponding scattering coefficients are consistent with those derived in the classical transfer matrix approach [54]. We also generalize our method to a resonator network, where multiple hanger- or necklace-type resonators are coupled in a chain with possible time delays. We reveal several interesting photon transport phenomena in such photonic-crystal-like systems and find consistency with the results reported in quantum optics. These results also indicate the possibility to generate high-quality modes from coupled low-quality resonators.

As a closing remark, we note that dephasing of microwave resonators can also be incorporated in the described formalism, which is, however, often neglected for linear resonators in the literature. To describe dephasing, we write the system-bath

interaction in the form [71–75]

$$H_{\text{int}} = \int_{-\infty}^{+\infty} d\omega \hbar a^\dagger (\kappa_\phi^* b_\omega^\dagger + \kappa_\phi b_\omega). \quad (87)$$

Here, b describes a general phase-damping bath, which may originate from the tunneling of atoms in the substrate between two bistable positions, or some parasitic source of mechanical modes, for example, the vibration of a dry cryostat. Then, the input-output relation can be readily derived by following the same procedure as described before. The result is

$$\dot{a} = -i\Delta a - \frac{\gamma_\phi}{2} a - \sqrt{\gamma_\phi} (ab_{\text{in}} - b_{\text{in}}^\dagger a), \quad (88)$$

where $\sqrt{\gamma_\phi} = i\sqrt{2\pi}\kappa_\phi$. We note that the input field $b_{\text{in}} = \int_{-\infty}^{+\infty} d\omega e^{+i\omega t} b_\omega(0)/\sqrt{2\pi}$ does not commute with the intraresonator field. However, the combined operators $b_{\text{in}} + (\sqrt{\gamma_\phi})^* a^\dagger/2$ and $b_{\text{in}}^\dagger + \sqrt{\gamma_\phi} a^\dagger/2$ commute with all the system operators [72], such that we rewrite Eq. (88) as

$$\dot{a} = -i\Delta a - \sqrt{\gamma_\phi} a (b_{\text{in}} - b_{\text{in}}^\dagger). \quad (89)$$

This result indicates that the input field b causes a random jittering to the resonant frequency of the intraresonator field a because any observation of the operator $(b_{\text{in}} - b_{\text{in}}^\dagger)$ is a purely imaginary number. Even though it conserves the energy of the system, the dephasing effect destroys the quantum coherence stored in the resonator and broadens the line shape of the scattering responses in a similar way of energy dissipation. One thus must resort to some extra measurements, for example, Ramsey interferometry, to distinguish the contributions of energy decay and dephasing from the line shape, instead of simply neglecting the dephasing effect. Today, high- Q superconducting microwave resonators with $Q_i > 10^6$ can be routinely made in the laboratory [76], while it remains a challenge for a decade to improve Q_i further. We anticipate that a

careful characterization of the dephasing rate may provide important insight on whether the state-of-the-art resonators are limited by energy dissipation or dephasing. This knowledge should pave a significant step towards making ultra-high- Q superconducting microwave resonators in the near future.

The Python codes for generating and analyzing the data of this study are available online [77].

ACKNOWLEDGMENTS

We acknowledge support by German Research Foundation via Germany's Excellence Strategy (Grant No. EXC-2111-390814868), Elite Network of Bavaria through the program ExQM, European Union via the Quantum Flagship project QMiCS (Project No. 820505), German Federal Ministry of Education and Research via the project QuaRaTe (Project No. 13N15380).

APPENDIX A: OUTLINE OF THE INPUT-OUTPUT ANALYSIS

We model a microwave resonator of any type as a composite system with the following Hamiltonian [59]:

$$H_{\text{sys}} = \sum_n \hbar \omega_n a_n^\dagger a_n, \quad (\text{A1})$$

$$H_{\text{bth}} = \sum_m \hbar \int_{-\infty}^{+\infty} d\omega \omega b_{m,\omega}^\dagger b_{m,\omega}, \quad (\text{A2})$$

$$H_{\text{int}} = \sum_{m,n} \hbar \int_{-\infty}^{+\infty} d\omega (\kappa_{m,n}^* a_n b_{m,\omega}^\dagger + \kappa_{m,n} a_n^\dagger b_{m,\omega}). \quad (\text{A3})$$

Following the Heisenberg equation, the time evolution of the intracavity field a_n as well as the bath field $b_{m,\omega}$ can be readily written as

$$\dot{a}_n = -i\omega_n a_n - i \sum_m \int_{-\infty}^{+\infty} d\omega \kappa_{m,n} b_m, \quad (\text{A4})$$

$$\dot{b}_m = -i\omega_l m - i \sum_n \kappa_{m,n}^* a_n. \quad (\text{A5})$$

By inserting the formal solution of Eq. (A5),

$$b_{m,\omega}(t) = e^{-i\omega(t-t_0)} b_{m,\omega}(t_0) - i \sum_n \kappa_{m,n}^* \int_{t_0}^t dt' e^{-i\omega(t-t')} a_n(t'), \quad (\text{A6})$$

into Eq. (A4), we obtain

$$\begin{aligned} \dot{a}_n = & -i\omega_n a_n - i \sum_m \kappa_{m,n} \int_{-\infty}^{+\infty} d\omega e^{-i\omega(t-t_0)} b_{m,\omega}(t_0) \\ & - \sum_{m,n'} \kappa_{m,n} \kappa_{m,n'}^* \int_{-\infty}^{+\infty} d\omega \int_{t_0}^t dt' e^{-i\omega(t-t')} a_n(t'). \end{aligned} \quad (\text{A7})$$

We recall the property that

$$\int_{-\infty}^{+\infty} d\omega e^{-i\omega(t-t_0)} = 2\pi \delta(t-t_0) \quad (\text{A8})$$

and define the input field, i.e., the noise operator in quantum Langevin equation, as

$$b_{m,\text{in}} = \frac{1}{\sqrt{2\pi}} \int_{-\infty}^{+\infty} d\omega e^{-i\omega(t-t_0)} b_{m,\omega}(t_0), \quad (\text{A9})$$

the dynamics of a_n can be simplified as

$$\dot{a}_n = -i\omega_n a_n - i \sum_m \sqrt{2\pi} \kappa_{m,n} b_{m,\text{in}} - \sum_{m,n'} \pi \kappa_{m,n} \kappa_{m,n'}^* a_n. \quad (\text{A10})$$

Alternatively, the formal solution of Eq. (A5) may be written as

$$\begin{aligned} b_{m,\omega}(t) = & e^{-i\omega(t-t_1)} b_{m,\omega}(t_1) \\ & + i \sum_n \kappa_{m,n}^* \int_{t_1}^t dt' e^{-i\omega(t-t')} a_n(t'), \end{aligned} \quad (\text{A11})$$

which gives

$$\begin{aligned} \dot{a}_n = & -i\omega_n a_n - i \sum_m \kappa_{m,n} \int_{-\infty}^{+\infty} d\omega e^{-i\omega(t-t_1)} b_{m,\omega}(t_1) \\ & + \sum_{m,n'} \kappa_{m,n} \kappa_{m,n'}^* \int_{-\infty}^{+\infty} d\omega \int_{t_1}^t dt' e^{-i\omega(t-t')} a_n(t'). \end{aligned} \quad (\text{A12})$$

We defined the output field as

$$b_{m,\text{out}} = \frac{1}{\sqrt{2\pi}} \int_{-\infty}^{+\infty} d\omega e^{-i\omega(t-t_1)} b_{m,\omega}(t_0), \quad (\text{A13})$$

such that the dynamics of a_n can be equivalently written as

$$\dot{a}_n = -i\omega_n a_n - i \sum_m \sqrt{2\pi} \kappa_{m,n} b_{m,\text{out}} + \sum_{m,n'} \pi \kappa_{m,n} \kappa_{m,n'}^* a_n. \quad (\text{A14})$$

Combining Eqs. (A9) and (A10) and (A13) and (A14), we obtain the so-called input-output relation [55,56]

$$\begin{aligned} \dot{a}_n = & -i\omega_n a_n - \sum_m \sqrt{\gamma_{m,n}} b_{m,\text{in}} \\ & - \frac{1}{2} \sum_{m,n'} \sqrt{\gamma_{m,n}} (\sqrt{\gamma_{m,n'}})^* a_n - \frac{\gamma_n}{2} a_n, \end{aligned} \quad (\text{A15})$$

$$b_{m,\text{out}} = b_{m,\text{in}} + \sum_{n'} (\sqrt{\gamma_{m,n'}})^* a_n. \quad (\text{A16})$$

Here, we have defined $\sqrt{\gamma_{m,n}} = i\sqrt{2\pi} \kappa_{m,n}$ and $(\sqrt{\gamma_{m,n}})^* = -i\sqrt{2\pi} \kappa_{m,n}^*$ and added the intrinsic damping of the intracavity modes by hand.

APPENDIX B: A CHAIN OF HANGER-TYPE RESONATORS WITH TIME DELAY

We consider a composite system where N hanger-type resonators are side coupled to a 1D waveguide. The system-bath interaction reads as

$$\begin{aligned} H_{\text{int}} = & \sum_{j=1}^N \int_{-\infty}^{+\infty} d\omega \hbar \{ e^{+i(j-1)\omega\tau} \kappa_j^* a_j^\dagger l_\omega^\dagger + e^{-i(j-1)\omega\tau} \kappa_j a_j^\dagger l_\omega \\ & + e^{-i(j-1)\omega\tau} \kappa_j^* a_j r_\omega^\dagger + e^{+i(j-1)\omega\tau} \kappa_j a_j^\dagger r_\omega \}. \end{aligned} \quad (\text{B1})$$

Here, we encode the information of the distance between different hanger-type resonators into a phase delay $l_\omega \rightarrow e^{-i(j-1)\omega\tau} l_\omega$, $r_\omega \rightarrow e^{+i(j-1)\omega\tau} r_\omega$ for $j = 1, \dots, N$. Following

the same procedure in Appendix A, we describe the dynamics of the intraresonator field a_j and the two bath fields l_ω and r_ω as

$$\begin{aligned} \dot{a}_j &= -i\Delta_j a_j - i\kappa_j \int_{-\infty}^{+\infty} d\omega e^{+i\omega(t-t_0)} e^{i(j-1)\omega\tau} l_\omega(t_0) - \sum_{j'} \kappa_j \kappa_{j'}^* \int_{-\infty}^{+\infty} d\omega \int_{t_0}^t dt' e^{+i\omega(t-t')} e^{i(j-j')\omega\tau} a_{n'}(t') \\ &\quad - i\kappa_j \int_{-\infty}^{+\infty} d\omega e^{-i\omega(t-t_0)} e^{i(j-1)\omega\tau} r_\omega(t_0) - \sum_{j'} \kappa_j \kappa_{j'}^* \int_{-\infty}^{+\infty} d\omega \int_{t_0}^t dt' e^{-i\omega(t-t')} e^{i(j-j')\omega\tau} a_{n'}(t'), \end{aligned} \quad (\text{B2})$$

$$l_\omega(t) = e^{-i\omega(t-t_0)} l_\omega(t_0) - i \sum_n e^{-i(j-1)\omega\tau} \kappa_{m,n}^* \int_{t_0}^t dt' e^{-i\omega(t-t')} a_{n'}(t'), \quad (\text{B3})$$

$$r_\omega(t) = e^{-i\omega(t-t_0)} r_\omega(t_0) - i \sum_n e^{-i(j-1)\omega\tau} \kappa_{m,n}^* \int_{t_0}^t dt' e^{-i\omega(t-t')} a_{n'}(t'). \quad (\text{B4})$$

We define the input fields as $l_{\text{in}} = (1/\sqrt{2\pi}) \int_{-\infty}^{+\infty} e^{-i\omega(t-t_0)} l_\omega(t_0) d\omega$ and $r_{\text{in}} = (1/\sqrt{2\pi}) \int_{-\infty}^{+\infty} e^{-i\omega(t-t_0)} r_\omega(t_0) d\omega$, such that Eq. (B2) can be written in a more compact form

$$\begin{aligned} \dot{a}_j &= -i\Delta_j a_j - 2\pi\kappa_j \kappa_j^* a_j - i\sqrt{2\pi}\kappa_j l_{\text{in}}[t + (j-1)\tau] - i\sqrt{2\pi}\kappa_j r_{\text{in}}[t - (j-1)\tau] \\ &\quad - 2\pi \sum_{j'>j} \kappa_j \kappa_{j'}^* a_{j'}[t + (j-j')\tau] - 2\pi \sum_{j'<j} \kappa_j \kappa_{j'}^* a_{j'}[t + (j'-j)\tau]. \end{aligned} \quad (\text{B5})$$

Here, a technical problem emerges that the time evolution of a_j involves operators at different times. To eliminate this time dependence, we note that the above analysis is performed in the rotating frame at the driving frequency ω_d . Thus, a time delay of τ in the operators may be fairly approximated by a phase factor $\exp(i\theta)$ with $\theta = \omega_d \tau$. In this regard, we rewrite Eq. (B5) as

$$\begin{aligned} \dot{a}_j &= -i\Delta_j a_j - 2\pi\kappa_j \kappa_j^* a_j - i\sqrt{2\pi}\kappa_j l_{\text{in}}(t) e^{-i(j-1)\theta} - i\sqrt{2\pi}\kappa_j r_{\text{in}}(t) e^{i(j-1)\theta} \\ &\quad - 2\pi \sum_{j'>j} \kappa_j \kappa_{j'}^* e^{(j'-j)\theta} a_{j'}(t) - 2\pi \sum_{j'<j} \kappa_j \kappa_{j'}^* e^{(j-j')\theta} a_{j'}(t). \end{aligned} \quad (\text{B6})$$

On the other hand, we have

$$\begin{aligned} \dot{a}_j &= -i\Delta_j a_j - i\kappa_j \int_{-\infty}^{+\infty} d\omega e^{+i\omega(t-t_1)} e^{i(j-1)\omega\tau} l_\omega(t_1) + \sum_{j'} \kappa_j \kappa_{j'}^* \int_{-\infty}^{+\infty} d\omega \int_t^{t_1} dt' e^{+i\omega(t-t')} e^{i(j-j')\omega\tau} a_{n'}(t') \\ &\quad - i\kappa_j \int_{-\infty}^{+\infty} d\omega e^{-i\omega(t-t_1)} e^{-i(j-1)\omega\tau} r_\omega(t_1) + \sum_{j'} \kappa_j \kappa_{j'}^* \int_{-\infty}^{+\infty} d\omega \int_t^{t_1} dt' e^{-i\omega(t-t')} e^{i(j-j')\omega\tau} a_{n'}(t'), \end{aligned} \quad (\text{B7})$$

$$l_\omega(t) = e^{+i\omega(t-t_1)} l_\omega(t_1) + i \sum_n e^{-i(j-1)\omega\tau} \kappa_{m,n}^* \int_t^{t_1} dt' e^{+i\omega(t-t')} a_{n'}(t'), \quad (\text{B8})$$

$$r_\omega(t) = e^{-i\omega(t-t_1)} r_\omega(t_1) + i \sum_n e^{-i(j-1)\omega\tau} \kappa_{m,n}^* \int_t^{t_1} dt' e^{-i\omega(t-t')} a_{n'}(t'). \quad (\text{B9})$$

We define the output fields as $l_{\text{out}} = (1/\sqrt{2\pi}) \int_{-\infty}^{+\infty} e^{+i\omega(t-t_1)} l_\omega(t_1) d\omega$, $r_{\text{out}} = (1/\sqrt{2\pi}) \int_{-\infty}^{+\infty} e^{+i\omega(t-t_1)} r_\omega(t_1) d\omega$, and repeat the above procedures. The result is

$$\begin{aligned} \dot{a}_j &= -i\Delta_j a_j + 2\pi\kappa_j \kappa_j^* a_j - i\sqrt{2\pi}\kappa_j l_{\text{out}}(t) e^{-i(j-1)\theta} - i\sqrt{2\pi}\kappa_j r_{\text{out}}(t) e^{i(j-1)\theta} \\ &\quad + 2\pi \sum_{j'<j} \kappa_j \kappa_{j'}^* e^{(j'-j)\theta} a_{j'}(t) + 2\pi \sum_{j'>j} \kappa_j \kappa_{j'}^* e^{(j-j')\theta} a_{j'}(t). \end{aligned} \quad (\text{B10})$$

Combining Eqs. (B6) and (B10), we obtain the input-output relations

$$l_{\text{out}} = l_{\text{in}} + \sqrt{2\pi}\kappa_j^* \sum_{j'=1}^N e^{i(j'-1)\theta} a_{j'}, \quad r_{\text{out}} = r_{\text{in}} + \sqrt{2\pi}\kappa_j^* \sum_{j'=1}^N e^{i(1-j')\theta} a_{j'}. \quad (\text{B11})$$

We note that the definition of input and output fields is different from that in Sec. III. To get the exact form, we redefine the operators l_{in} and r_{in} as the input fields at the right and left sides of the waveguide, and l_{out} and r_{out} as the output fields at the left

and right sides. In other words, we perform the transform $l_{\text{in}} \rightarrow e^{i(N-1)\theta} l_{\text{in}}$, $r_{\text{out}} \rightarrow e^{-i(N-1)\theta} r_{\text{out}}$. The new input-output relations are

$$\dot{a}_j = -i\Delta_j a_j - \sum_{j'=1}^N \sqrt{\gamma_j} (\sqrt{\gamma_{j'}})^* e^{i|j'-j|\theta} a_{j'}(t) - \sqrt{\gamma_j} l_{\text{in}}(t) e^{-i(j-N)\theta} - \sqrt{\gamma_j} r_{\text{in}}(t) e^{i(j-1)\theta}, \quad (\text{B12})$$

$$l_{\text{out}} = e^{i(N-1)\theta} l_{\text{in}} + \sum_{j'=1}^N (\sqrt{\gamma_{j'}})^* e^{i(j'-1)\theta} a_j, \quad (\text{B13})$$

$$r_{\text{out}} = e^{i(N-1)\theta} r_{\text{in}} + \sum_{j'=1}^N (\sqrt{\gamma_{j'}})^* e^{i(N-j')\theta} a_j. \quad (\text{B14})$$

Correspondingly, the scattering coefficients read as

$$S_{11} = \frac{\langle l_{\text{out}} \rangle}{\langle r_{\text{in}} \rangle}, \quad S_{21} = \frac{\langle r_{\text{out}} \rangle}{\langle r_{\text{in}} \rangle} \text{ with } \langle l_{\text{in}} \rangle = 0, \quad \text{and } S_{12} = \frac{\langle l_{\text{out}} \rangle}{\langle l_{\text{in}} \rangle}, \quad S_{22} = \frac{\langle r_{\text{out}} \rangle}{\langle l_{\text{in}} \rangle} \text{ with } \langle r_{\text{in}} \rangle = 0. \quad (\text{B15})$$

For the simplicity of calculation, we define

$$c_j = \sum_{j' \geq j} (\sqrt{\gamma_{j'}})^* e^{ij'\theta} a_{j'}, \quad d_j = \sum_{j' \leq j} (\sqrt{\gamma_{j'}})^* e^{-ij'\theta} a_{j'}, \quad (\text{B16})$$

such that the input-output relation can be written in a compact form

$$l_{\text{out}} = e^{i(N-1)\theta} l_{\text{in}} + e^{-i\theta} c_1, \quad (\text{B17})$$

$$r_{\text{out}} = e^{i(N-1)\theta} r_{\text{in}} + e^{iN\theta} d_N. \quad (\text{B18})$$

On the other hand, the steady-state solution of intracavity field a_j reads as

$$(i\Delta_j - \gamma_j + \frac{\gamma_{a,j}}{2}) a_j = -e^{-ij\theta} \sqrt{\gamma_j} c_j - e^{+ij\theta} \sqrt{\gamma_j} d_j - \sqrt{\gamma_j} l_{\text{in}}(t) e^{-i(j-N)\theta} - \sqrt{\gamma_j} r_{\text{in}}(t) e^{i(j-1)\theta}, \quad (\text{B19})$$

and thus

$$c_j = \sum_{j' \geq j} -\frac{\gamma_{j'}}{i\Delta_{j'} - \gamma_{j'} + \frac{\gamma_{a,j'}}{2}} (c_{j'} + e^{+i2j'\theta} d_{j'} + e^{+iN\theta} l_{\text{in}} + e^{i(2j'-1)\theta} r_{\text{in}}), \quad (\text{B20})$$

$$d_j = \sum_{j' \leq j} -\frac{\gamma_{j'}}{i\Delta_{j'} - \gamma_{j'} + \frac{\gamma_{a,j'}}{2}} (e^{-i2j'\theta} c_{j'} + d_{j'} + e^{+i(N-2j')\theta} l_{\text{in}} + e^{-i\theta} r_{\text{in}}). \quad (\text{B21})$$

In these regards, one can readily obtain the input-output relations by solving a linear equation.

APPENDIX C: NUMERICAL SOLUTION FOR A HOMOGENEOUS HANGER-TYPE-RESONATOR CHAIN

Let us now derive an analytical expression for the scattering coefficients for the special case where $\gamma_j \equiv \gamma$, $\gamma_{a,j} \equiv \gamma_a$, $\Delta_j \equiv \Delta$. We define

$$c_j = \sum_{j' \geq j} (\sqrt{\gamma})^* e^{ij'\theta} a_{j'}, \quad d_j = \sum_{j' \leq j} (\sqrt{\gamma})^* e^{-ij'\theta} a_{j'}, \quad (\text{C1})$$

such that the steady-state solution of Eq. (B19) can be written as

$$a_j = -\frac{e^{-ij\theta} \sqrt{\gamma}}{i\Delta - \gamma + \frac{\gamma_a}{2}} c_j - \frac{e^{+ij\theta} \sqrt{\gamma}}{i\Delta - \gamma + \frac{\gamma_a}{2}} d_j - \frac{e^{-i(j-N)\theta} \sqrt{\gamma}}{i\Delta - \gamma + \frac{\gamma_a}{2}} l_{\text{in}} - \frac{e^{i(j-1)\theta} \sqrt{\gamma}}{i\Delta - \gamma + \frac{\gamma_a}{2}} r_{\text{in}}. \quad (\text{C2})$$

By combining Eqs. (C1) and (C2), we obtain a set of linear equations

$$x e^{-i2\theta} c_1 + (x+1) d_1 + x(e^{+i(N-2)\theta} l_{\text{in}} + e^{-i\theta} r_{\text{in}}) = 0, \quad (\text{C3})$$

$$x e^{-i2(j+1)\theta} c_{j+1} - d_j + (x+1) d_{j+1} + x(e^{+i(N-2(j+1))\theta} l_{\text{in}} + e^{-i\theta} r_{\text{in}}) = 0, \quad (\text{C4})$$

$$(x+1) c_j - c_{j+1} + x e^{+i2j\theta} d_j + x(e^{+iN\theta} l_{\text{in}} + e^{i(2j-1)\theta} r_{\text{in}}) = 0, \quad (\text{C5})$$

$$(x+1) c_N + x e^{+i2N\theta} d_N + x(e^{+iN\theta} l_{\text{in}} + e^{i(2N-1)\theta} r_{\text{in}}) = 0, \quad (\text{C6})$$

where we have defined $x = \gamma/(i\Delta - \gamma + \gamma_a/2)$ for convenience. Next, we decouple the variables c_j and d_j and obtain the following two sets of linear equations:

$$-\frac{(1+2x)}{x}c_1 + \frac{(1+x)}{x}c_2 - e^{iN\theta}l_{\text{in}} - e^{i\theta}r_{\text{in}} = 0, \quad (\text{C7})$$

$$\frac{(x+1)e^{i2\theta}}{x}c_{j-1} - \frac{(1+2x+e^{i2\theta})}{x}c_j + \frac{(1+x)}{x}c_{j+1} + e^{iN\theta}(e^{i2\theta}-1)l_{\text{in}} = 0, \quad j = 2, \dots, N-1 \quad (\text{C8})$$

$$\frac{(x+1)e^{i2\theta}}{x}c_{N-1} - \frac{(1+2x+e^{i2\theta})}{x}c_N + e^{iN\theta}(e^{i2\theta}-1)l_{\text{in}} = 0, \quad (\text{C9})$$

$$-\frac{(1+e^{i2\theta}+2x)}{x}d_1 + \frac{e^{i2\theta}(x+1)}{x}d_2 + (e^{i\theta}-e^{-i\theta})r_{\text{in}} = 0, \quad (\text{C10})$$

$$\frac{(1+x)}{x}d_{j-1} - \frac{(1+e^{i2\theta}+2x)}{x}d_j + \frac{e^{i2\theta}(x+1)}{x}d_{j+1} + (e^{i\theta}-e^{-i\theta})r_{\text{in}} = 0, \quad j = 2, \dots, N-1 \quad (\text{C11})$$

$$\frac{(1+x)}{x}d_{N-1} - \frac{(1+2x)}{x}d_N - e^{-iN\theta}l_{\text{in}} - e^{-i\theta}r_{\text{in}} = 0. \quad (\text{C12})$$

In the matrix form $Ax = 0$, the above equations indicate that A is tridiagonal such that x can be efficiently solved by using the so-called Thomas or TDMA algorithm. That is $c_N = z_N$, $c_j = z_j - y_j c_{j+1}$ for $j = N-1, \dots, 1$, where

$$y_j = \begin{cases} -\frac{1+x}{1+2x}, & j = 1 \\ -\frac{1+x}{(1+2x+e^{i2\theta})+y_{j-1}(1+x)e^{i2\theta}}, & j = 2, \dots, N-1 \end{cases}, \quad z_j = \begin{cases} -\frac{x(e^{iN\theta}l_{\text{in}}+e^{i\theta}r_{\text{in}})}{1+2x}, & j = 1 \\ -\frac{xe^{iN\theta}(1-e^{i2\theta})l_{\text{in}}-z_{j-1}(1+x)e^{i2\theta}}{(1+2x+e^{i2\theta})+y_{j-1}(1+x)e^{i2\theta}}, & j = 2, \dots, N-1. \end{cases} \quad (\text{C13})$$

Or, $d_1 = z_N$, $d_{N-j+1} = z_j - y_j d_{N-j}$ for $j = N-1, \dots, 1$, where

$$y_j = \begin{cases} -\frac{1+x}{1+2x}, & j = 1 \\ -\frac{1+x}{(1+2x+e^{i2\theta})+y_{j-1}(1+x)e^{i2\theta}}, & j = 2, \dots, N-1 \end{cases}, \quad z_j = \begin{cases} -\frac{x(e^{-iN\theta}l_{\text{in}}+e^{-i\theta}r_{\text{in}})}{1+2x}, & j = 1 \\ -\frac{x(e^{-i\theta}-e^{i\theta})r_{\text{in}}-z_{j-1}(1+x)e^{i2\theta}}{(1+2x+e^{i2\theta})+y_{j-1}(1+x)e^{i2\theta}}, & j = 2, \dots, N-1. \end{cases} \quad (\text{C14})$$

APPENDIX D: A CHAIN OF NECKLACE-TYPE RESONATORS WITH TWO BOUNDARY CONDITIONS

We consider a chain of necklace-type resonators. For hard-wall boundary conditions, we define

$$d_1 = \sum_{k'=1}^N \sqrt{\gamma_{1,k'}} c_{k'}, \quad d_2 = \sum_{k'=1}^N (-1)^{k'} \sqrt{\gamma_{2,k'}} c_{k'}, \quad (\text{D1})$$

such that, for steady-state solutions, we have

$$c_k = -\frac{\frac{1}{2}\sqrt{\gamma_{1,k}}d_1 + \frac{(-1)^k}{2}\sqrt{\gamma_{2,k}}d_2 + \sqrt{\gamma_{1,k}}b_{1,\text{in}} + (-1)^k\sqrt{\gamma_{2,k}}b_{2,\text{in}}}{i\Delta_k + \frac{\gamma_a}{2}}. \quad (\text{D2})$$

We note that c_k is defined as the collective mode of the resonator chain. Combining Eqs. (D1) and (D2), we obtain

$$d_1 = -\sum_{k=1}^N \frac{\frac{1}{2}\gamma_{1,k}d_1 + \frac{(-1)^k}{2}\sqrt{\gamma_{1,k}\gamma_{2,k}}d_2 + \gamma_{1,k}b_{1,\text{in}} + (-1)^k\sqrt{\gamma_{1,k}\gamma_{2,k}}b_{2,\text{in}}}{i\Delta_k + \frac{\gamma_a}{2}}, \quad (\text{D3})$$

$$d_2 = -\sum_{k=1}^N \frac{\frac{(-1)^k}{2}\sqrt{\gamma_{1,k}\gamma_{2,k}}d_1 + \frac{1}{2}\gamma_{2,k}d_2 + (-1)^k\sqrt{\gamma_{1,k}\gamma_{2,k}}b_{1,\text{in}} + \gamma_{2,k}b_{2,\text{in}}}{i\Delta_k + \frac{\gamma_a}{2}}. \quad (\text{D4})$$

The solutions of d_1 and d_2 read as

$$d_1 = -\frac{\left[\left(1 + \frac{1}{2} \sum_{k=1}^N \frac{\gamma_{2,k}}{i\Delta_k + \frac{\gamma_a}{2}}\right) \left(\sum_{k=1}^N \frac{\gamma_{1,k}}{i\Delta_k + \frac{\gamma_a}{2}}\right) - \frac{1}{2} \left(\sum_{k=1}^N \frac{(-1)^k \sqrt{\gamma_{1,k}\gamma_{2,k}}}{i\Delta_k + \frac{\gamma_a}{2}}\right)^2 \right] b_{1,\text{in}} + \left(\sum_{k=1}^N \frac{(-1)^k \sqrt{\gamma_{1,k}\gamma_{2,k}}}{i\Delta_k + \frac{\gamma_a}{2}}\right) b_{2,\text{in}}}{\left(1 + \frac{1}{2} \sum_{k=1}^N \frac{\gamma_{1,k}}{i\Delta_k + \frac{\gamma_a}{2}}\right) \left(1 + \frac{1}{2} \sum_{k=1}^N \frac{\gamma_{2,k}}{i\Delta_k + \frac{\gamma_a}{2}}\right) - \left(\frac{1}{2} \sum_{k=1}^N \frac{(-1)^k \sqrt{\gamma_{1,k}\gamma_{2,k}}}{i\Delta_k + \frac{\gamma_a}{2}}\right)^2}, \quad (\text{D5})$$

$$d_2 = -\frac{\left(\sum_{k=1}^N \frac{(-1)^k \sqrt{\gamma_{1,k}\gamma_{2,k}}}{i\Delta_k + \frac{\gamma_a}{2}}\right) b_{1,\text{in}} + \left[\left(1 + \frac{1}{2} \sum_{k=1}^N \frac{\gamma_{1,k}}{i\Delta_k + \frac{\gamma_a}{2}}\right) \left(\sum_{k=1}^N \frac{\gamma_{2,k}}{i\Delta_k + \frac{\gamma_a}{2}}\right) - \frac{1}{2} \left(\sum_{k=1}^N \frac{(-1)^k \sqrt{\gamma_{1,k}\gamma_{2,k}}}{i\Delta_k + \frac{\gamma_a}{2}}\right)^2 \right] b_{2,\text{in}}}{\left(1 + \frac{1}{2} \sum_{k=1}^N \frac{\gamma_{1,k}}{i\Delta_k + \frac{\gamma_a}{2}}\right) \left(1 + \frac{1}{2} \sum_{k=1}^N \frac{\gamma_{2,k}}{i\Delta_k + \frac{\gamma_a}{2}}\right) - \left(\frac{1}{2} \sum_{k=1}^N \frac{(-1)^k \sqrt{\gamma_{1,k}\gamma_{2,k}}}{i\Delta_k + \frac{\gamma_a}{2}}\right)^2}. \quad (\text{D6})$$

Thus, the input-output relations can be readily obtained by inserting d_1 and d_2 into Eqs. (A15) and (A16).

For periodic boundary conditions, we define

$$d_1 = \sum_{k'=1}^N \sqrt{\gamma_{1,k'}} c_{k'}, \quad d_2 = - \sum_{k'=1}^N \sqrt{\gamma_{2,k'}} c_{k'}, \quad (\text{D7})$$

such that

$$c_k = - \frac{\frac{1}{2} \sqrt{\gamma_{1,k}} d_1 - \frac{1}{2} \sqrt{\gamma_{2,k}} d_2 + \sqrt{\gamma_{1,k}} b_{1,\text{in}} - \sqrt{\gamma_{2,k}} b_{2,\text{in}}}{i \Delta_k + \frac{\gamma_a}{2}}. \quad (\text{D8})$$

Combining Eqs. (D7) and (D8), we obtain

$$d_1 = - \sum_{k=1}^N \frac{\frac{1}{2} \gamma_{1,k} d_1 - \frac{1}{2} \sqrt{\gamma_{1,k} \gamma_{2,k}} d_2 + \gamma_{1,k} b_{1,\text{in}} - \sqrt{\gamma_{1,k} \gamma_{2,k}} b_{2,\text{in}}}{i \Delta_k + \frac{\gamma_a}{2}}, \quad (\text{D9})$$

$$d_2 = - \sum_{k=1}^N \frac{-\frac{1}{2} \sqrt{\gamma_{1,k} \gamma_{2,k}} d_1 + \frac{1}{2} \gamma_{2,k} d_2 - \sqrt{\gamma_{1,k} \gamma_{2,k}} b_{1,\text{in}} + \gamma_{2,k} b_{2,\text{in}}}{i \Delta_k + \frac{\gamma_a}{2}}. \quad (\text{D10})$$

The solutions of d_1 and d_2 read as

$$d_1 = \frac{- \left[\left(1 + \frac{1}{2} \sum_{k=1}^N \frac{\gamma_{2,k}}{i \Delta_k + \frac{\gamma_a}{2}} \right) \left(\sum_{k=1}^N \frac{\gamma_{1,k}}{i \Delta_k + \frac{\gamma_a}{2}} \right) - \frac{1}{2} \left(\sum_{k=1}^N \frac{\sqrt{\gamma_{1,k} \gamma_{2,k}}}{i \Delta_k + \frac{\gamma_a}{2}} \right)^2 \right] b_{1,\text{in}} + \left(\sum_{k=1}^N \frac{\sqrt{\gamma_{1,k} \gamma_{2,k}}}{i \Delta_k + \frac{\gamma_a}{2}} \right) b_{2,\text{in}}}{\left(1 + \frac{1}{2} \sum_{k=1}^N \frac{\gamma_{1,k}}{i \Delta_k + \frac{\gamma_a}{2}} \right) \left(1 + \frac{1}{2} \sum_{k=1}^N \frac{\gamma_{2,k}}{i \Delta_k + \frac{\gamma_a}{2}} \right) - \left(\frac{1}{2} \sum_{k=1}^N \frac{\sqrt{\gamma_{1,k} \gamma_{2,k}}}{i \Delta_k + \frac{\gamma_a}{2}} \right)^2}, \quad (\text{D11})$$

$$d_2 = \frac{\left(\sum_{k=1}^N \frac{\sqrt{\gamma_{1,k} \gamma_{2,k}}}{i \Delta_k + \frac{\gamma_a}{2}} \right) b_{1,\text{in}} - \left[\left(1 + \frac{1}{2} \sum_{k=1}^N \frac{\gamma_{1,k}}{i \Delta_k + \frac{\gamma_a}{2}} \right) \left(\sum_{k=1}^N \frac{\gamma_{2,k}}{i \Delta_k + \frac{\gamma_a}{2}} \right) - \frac{1}{2} \left(\sum_{k=1}^N \frac{\sqrt{\gamma_{1,k} \gamma_{2,k}}}{i \Delta_k + \frac{\gamma_a}{2}} \right)^2 \right] b_{2,\text{in}}}{\left(1 + \frac{1}{2} \sum_{k=1}^N \frac{\gamma_{1,k}}{i \Delta_k + \frac{\gamma_a}{2}} \right) \left(1 + \frac{1}{2} \sum_{k=1}^N \frac{\gamma_{2,k}}{i \Delta_k + \frac{\gamma_a}{2}} \right) - \left(\frac{1}{2} \sum_{k=1}^N \frac{\sqrt{\gamma_{1,k} \gamma_{2,k}}}{i \Delta_k + \frac{\gamma_a}{2}} \right)^2}. \quad (\text{D12})$$

Similarly, the input-output relations can be obtained by inserting d_1 and d_2 into Eqs. (A15) and (A16).

-
- [1] X. Gu, A. F. Kockum, A. Miranowicz, Y.-x. Liu, and F. Nori, Microwave photonics with superconducting quantum circuits, *Phys. Rep.* **718-719**, 1 (2017).
- [2] A. Blais, R.-S. Huang, A. Wallraff, S. M. Girvin, and R. J. Schoelkopf, Cavity quantum electrodynamics for superconducting electrical circuits: An architecture for quantum computation, *Phys. Rev. A* **69**, 062320 (2004).
- [3] A. Wallraff, D. I. Schuster, A. Blais, L. Frunzio, R.-S. Huang, J. Majer, S. Kumar, S. M. Girvin, and R. J. Schoelkopf, Strong coupling of a single photon to a superconducting qubit using circuit quantum electrodynamics, *Nature (London)* **431**, 162 (2004).
- [4] J.-T. Shen and S. Fan, Coherent Single Photon Transport in a One-Dimensional Waveguide Coupled with Superconducting Quantum Bits, *Phys. Rev. Lett.* **95**, 213001 (2005); Coherent photon transport from spontaneous emission in one-dimensional waveguides, *Opt. Lett.* **30**, 2001 (2005).
- [5] V. Bužek, G. Drobný, M. G. Kim, M. Havukainen, and P. L. Knight, Numerical simulations of atomic decay in cavities and material media, *Phys. Rev. A* **60**, 582 (1999).
- [6] L. Zhou, Z. R. Gong, Y.-x. Liu, C. P. Sun, and F. Nori, Controllable Scattering of a Single Photon inside a One-Dimensional Resonator Waveguide, *Phys. Rev. Lett.* **101**, 100501 (2008).
- [7] J.-T. Shen and S. Fan, Theory of single-photon transport in a single-mode waveguide. I. Coupling to a cavity containing a two-level atom, *Phys. Rev. A* **79**, 023837 (2009); Theory of single-photon transport in a single-mode waveguide. II. Coupling to a whispering-gallery resonator containing a two-level atom, *Phys. Rev. A* **79**, 023838 (2009).
- [8] O. Astafiev, A. M. Zagoskin, A. A. Abdumalikov Jr., Y. A. Pashkin, T. Yamamoto, K. Inomata, Y. Nakamura, and J. S. Tsai, Resonance fluorescence of a single artificial atom, *Science* **327**, 840 (2010).
- [9] J.-Q. Liao and C. K. Law, Correlated two-photon transport in a one-dimensional waveguide side-coupled to a nonlinear cavity, *Phys. Rev. A* **82**, 053836 (2010).
- [10] D. Zueco, J. J. Mazo, E. Solano, and J. J. García-Ripoll, Microwave photonics with josephson junction arrays: Negative refraction index and entanglement through disorder, *Phys. Rev. B* **86**, 024503 (2012).
- [11] K. Lalumière, B. C. Sanders, A. F. van Loo, A. Fedorov, A. Wallraff, and A. Blais, Input-output theory for waveguide QED with an ensemble of inhomogeneous atoms, *Phys. Rev. A* **88**, 043806 (2013).
- [12] A. F. van Loo, A. Fedorov, K. Lalumiere, B. C. Sanders, A. Blais, and A. Wallraff, Photon-mediated interactions between distant artificial atoms, *Science* **342**, 1494 (2013).
- [13] H. Pichler and P. Zoller, Photonic Circuits with Time Delays and Quantum Feedback, *Phys. Rev. Lett.* **116**, 093601 (2016).
- [14] J.-F. Huang, J.-Q. Liao, and C. P. Sun, Photon blockade induced by atoms with Rydberg coupling, *Phys. Rev. A* **87**, 023822 (2013).
- [15] Q. Li, L. Zhou, and C. P. Sun, Waveguide quantum electrodynamics: Controllable channel from quantum interference, *Phys. Rev. A* **89**, 063810 (2014).

- [16] X. Gu, S.-N. Huai, F. Nori, and Y.-x. Liu, Polariton states in circuit QED for electromagnetically induced transparency, *Phys. Rev. A* **93**, 063827 (2016).
- [17] J. Long, H. S. Ku, X. Wu, X. Gu, R. E. Lake, M. Bal, Y.-x. Liu, and D. P. Pappas, Electromagnetically Induced Transparency in Circuit Quantum Electrodynamics with Nested Polariton States, *Phys. Rev. Lett.* **120**, 083602 (2018).
- [18] W. Nie, Z. H. Peng, F. Nori, and Y.-x. Liu, Topologically Protected Quantum Coherence in a Superatom, *Phys. Rev. Lett.* **124**, 023603 (2020).
- [19] W. Nie and Y. X. Liu, Bandgap-assisted quantum control of topological edge states in a cavity, *Phys. Rev. Res.* **2**, 012076(R) (2020).
- [20] S. Fan, Sharp asymmetric line shapes in side-coupled waveguide-cavity systems, *Appl. Phys. Lett.* **80**, 908 (2002).
- [21] A. Chiba, H. Fujiwara, J.-i. Hotta, S. Takeuchi, and K. Sasaki, Fano resonance in a multimode tapered fiber coupled with a microspherical cavity, *Appl. Phys. Lett.* **86**, 261106 (2005).
- [22] P. Chak, S. Pereira, and J. E. Sipe, Coupled-mode theory for periodic side-coupled microcavity and photonic crystal structures, *Phys. Rev. B* **73**, 035105 (2006).
- [23] Y.-F. Xiao, M. Li, Y.-C. Liu, Y. Li, X. Sun, and Q. Gong, Asymmetric Fano resonance analysis in indirectly coupled microresonators, *Phys. Rev. A* **82**, 065804 (2010).
- [24] S. Longhi, Tunable dynamic Fano resonances in coupled-resonator optical waveguides, *Phys. Rev. A* **91**, 063809 (2015).
- [25] S. John and J. Wang, Quantum optics of localized light in a photonic band gap, *Phys. Rev. B* **43**, 12772 (1991).
- [26] M. Notomi, K. Yamada, A. Shinya, J. Takahashi, C. Takahashi, and I. Yokohama, Extremely Large Group-Velocity Dispersion of Line-Defect Waveguides in Photonic Crystal Slabs, *Phys. Rev. Lett.* **87**, 253902 (2001); M. Notomi, E. Kuramochi, and T. Tanabe, Large-scale arrays of ultrahigh-q coupled nanocavities, *Nat. Photonics* **2**, 741 (2008).
- [27] M. F. Yanik and S. Fan, Stopping Light All Optically, *Phys. Rev. Lett.* **92**, 083901 (2004); M. F. Yanik, W. Suh, Z. Wang, and S. Fan, Stopping Light in a Waveguide with an All-Optical Analog of Electromagnetically Induced Transparency, *ibid.* **93**, 233903 (2004); M. F. Yanik and S. Fan, Stopping and storing light coherently, *Phys. Rev. A* **71**, 013803 (2005).
- [28] Q. Xu, P. Dong, and M. Lipson, Breaking the delay-bandwidth limit in a photonic structure, *Nat. Phys.* **3**, 406 (2007).
- [29] Y. Dumeige, S. Trebaol, and P. Féron, Intracavity coupled-active-resonator-induced dispersion, *Phys. Rev. A* **79**, 013832 (2009).
- [30] D. D. Smith, H. Chang, K. A. Fuller, A. T. Rosenberger, and R. W. Boyd, Coupled-resonator-induced transparency, *Phys. Rev. A* **69**, 063804 (2004).
- [31] K. Totsuka, N. Kobayashi, and M. Tomita, Slow Light in Coupled-Resonator-Induced Transparency, *Phys. Rev. Lett.* **98**, 213904 (2007).
- [32] Y.-F. Xiao, X.-B. Zou, W. Jiang, Y.-L. Chen, and G.-C. Guo, Analog to multiple electromagnetically induced transparency in all-optical drop-filter systems, *Phys. Rev. A* **75**, 063833 (2007).
- [33] X. Yang, M. Yu, D.-L. Kwong, and C. W. Wong, All-Optical Analog to Electromagnetically Induced Transparency in Multiple Coupled Photonic Crystal Cavities, *Phys. Rev. Lett.* **102**, 173902 (2009).
- [34] E. N. Bulgakov and A. F. Sadreev, Bound states in the continuum in photonic waveguides inspired by defects, *Phys. Rev. B* **78**, 075105 (2008).
- [35] T. Shi and C. P. Sun, Lehmann-Symanzik-Zimmermann reduction approach to multiphoton scattering in coupled-resonator arrays, *Phys. Rev. B* **79**, 205111 (2009).
- [36] P. Longo, P. Schmitteckert, and K. Busch, Few-Photon Transport in Low-Dimensional Systems: Interaction-Induced Radiation Trapping, *Phys. Rev. Lett.* **104**, 023602 (2010).
- [37] M. Biondi, S. Schmidt, G. Blatter, and H. E. Türeci, Self-protected polariton states in photonic quantum metamaterials, *Phys. Rev. A* **89**, 025801 (2014).
- [38] A. Biella, L. Mazza, I. Carusotto, D. Rossini, and R. Fazio, Photon transport in a dissipative chain of nonlinear cavities, *Phys. Rev. A* **91**, 053815 (2015).
- [39] L. Qiao and C.-P. Sun, Atom-photon bound states and non-markovian cooperative dynamics in coupled-resonator waveguides, *Phys. Rev. A* **100**, 063806 (2019).
- [40] N. M. Sundaresan, R. Lundgren, G. Zhu, A. V. Gorshkov, and A. A. Houck, Interacting Qubit-Photon Bound States with Superconducting Circuits, *Phys. Rev. X* **9**, 011021 (2019).
- [41] S. Fan, S. E. Kocabaş, and J.-T. Shen, Input-output formalism for few-photon transport in one-dimensional nanophotonic waveguides coupled to a qubit, *Phys. Rev. A* **82**, 063821 (2010); S. Xu and S. Fan, Input-output formalism for few-photon transport: A systematic treatment beyond two photons, *ibid.* **91**, 043845 (2015).
- [42] A. Yariv, Y. Xu, R. K. Lee, and A. Scherer, Coupled-resonator optical waveguide: A proposal and analysis, *Opt. Lett.* **24**, 711 (1999); Y. Xu, Y. Li, R. K. Lee, and A. Yariv, Scattering-theory analysis of waveguide-resonator coupling, *Phys. Rev. E* **62**, 7389 (2000).
- [43] M. Pierre, S. R. Sathyamoorthy, I.-M. Svensson, G. Johansson, and P. Delsing, Resonant and off-resonant microwave signal manipulation in coupled superconducting resonators, *Phys. Rev. B* **99**, 094518 (2019).
- [44] J. Leppäkangas, J. D. Brehm, P. Yang, L. Guo, M. Marthaler, A. V. Ustinov, and M. Weides, Resonance inversion in a superconducting cavity coupled to artificial atoms and a microwave background, *Phys. Rev. A* **99**, 063804 (2019).
- [45] C. W. Gardiner, Driving a Quantum System with the Output Field from Another Driven Quantum System, *Phys. Rev. Lett.* **70**, 2269 (1993).
- [46] H. J. Carmichael, Quantum Trajectory Theory for Cascaded Open Systems, *Phys. Rev. Lett.* **70**, 2273 (1993).
- [47] J. I. Cirac, P. Zoller, H. J. Kimble, and H. Mabuchi, Quantum State Transfer and Entanglement Distribution among Distant Nodes in a Quantum Network, *Phys. Rev. Lett.* **78**, 3221 (1997).
- [48] J. Gough and M. James, The series product and its application to quantum feedforward and feedback networks, *IEEE Trans. Autom. Control* **54**, 2530 (2009).
- [49] J. Combes, J. Kerckhoff, and M. Sarovar, The SLH framework for modeling quantum input-output networks, *Adv. Phys.:X* **2**, 784 (2017).
- [50] A. H. Kiielerich and K. Mølmer, Input-Output Theory with Quantum Pulses, *Phys. Rev. Lett.* **123**, 123604 (2019).
- [51] A. Yariv, Coupled-mode theory for guided-wave optics, *IEEE J. Quantum Electron.* **9**, 919 (1973).

- [52] H. Haus and W. Huang, Coupled-mode theory, *Proc. IEEE* **79**, 1505 (1991).
- [53] J. Heinsoo, C. K. Andersen, A. Remm, S. Krinner, T. Walter, Y. Salathé, S. Gasparinetti, J.-C. Besse, A. Potočnik, A. Wallraff, and C. Eichler, Rapid High-Fidelity Multiplexed Readout of Superconducting Qubits, *Phys. Rev. Appl.* **10**, 034040 (2018).
- [54] Q.-M. Chen, M. Pfeiffer, M. Partanen, F. Fesquet, K. E. Honasoge, F. Kronowetter, Y. Nojiri, M. Renger, K. G. Fedorov, A. Marx, F. Deppe, and R. Gross, Scattering coefficients of superconducting microwave resonators. I. Transfer matrix approach *Phys. Rev. B* **106**, 214505 (2022).
- [55] M. J. Collett and C. W. Gardiner, Squeezing of intracavity and traveling-wave light fields produced in parametric amplification, *Phys. Rev. A* **30**, 1386 (1984).
- [56] C. W. Gardiner and M. J. Collett, Input and output in damped quantum systems: Quantum stochastic differential equations and the master equation, *Phys. Rev. A* **31**, 3761 (1985).
- [57] J. M. Fink, L. Steffen, P. Studer, L. S. Bishop, M. Baur, R. Bianchetti, D. Bozyigit, C. Lang, S. Filipp, P. J. Leek, and A. Wallraff, Quantum-To-Classical Transition in Cavity Quantum Electrodynamics, *Phys. Rev. Lett.* **105**, 163601 (2010).
- [58] S. M. Girvin, Circuit QED: Superconducting qubits coupled to microwave photons, in *Quantum Machines: Measurement and Control of Engineered Quantum Systems*, edited by M. Devoret, B. Huard, R. Schoelkopf, and L. F. Cugliandolo (Oxford University Press, Oxford, 2011), pp. 113–256.
- [59] H. J. Carmichael, *Statistical Methods in Quantum Optics I: Master Equations and Fokker-Planck Equations* (Springer, New York, 2013).
- [60] G. Breit and E. Wigner, Capture of slow neutrons, *Phys. Rev.* **49**, 519 (1936).
- [61] A. E. Miroshnichenko, S. Flach, and Y. S. Kivshar, Fano resonances in nanoscale structures, *Rev. Mod. Phys.* **82**, 2257 (2010).
- [62] M. Fischer, Q.-M. Chen, C. Besson, P. Eder, J. Goetz, S. Pogorzalek, M. Renger, E. Xie, M. J. Hartmann, K. G. Fedorov, A. Marx, F. Deppe, and R. Gross, In situ tunable nonlinearity and competing signal paths in coupled superconducting resonators, *Phys. Rev. B* **103**, 094515 (2021).
- [63] A. Wójcik, T. Łuczak, P. Kurzyński, A. Grudka, T. Gdala, and M. Bednarska, Unmodulated spin chains as universal quantum wires, *Phys. Rev. A* **72**, 034303 (2005); Multiuser quantum communication networks, *Phys. Rev. A* **75**, 022330 (2007).
- [64] J.-Q. Liao, J.-F. Huang, Y.-x. Liu, L.-M. Kuang, and C. P. Sun, Quantum switch for single-photon transport in a coupled superconducting transmission-line-resonator array, *Phys. Rev. A* **80**, 014301 (2009).
- [65] J.-Q. Liao, Z. R. Gong, L. Zhou, Y.-x. Liu, C. P. Sun, and F. Nori, Controlling the transport of single photons by tuning the frequency of either one or two cavities in an array of coupled cavities, *Phys. Rev. A* **81**, 042304 (2010).
- [66] M. Sumetsky and B. Eggleton, Modeling and optimization of complex photonic resonant cavity circuits, *Opt. Express* **11**, 381 (2003).
- [67] Y. Hara, T. Mukaiyama, K. Takeda, and M. Kuwata-Gonokami, Heavy Photon States in Photonic Chains of Resonantly Coupled Cavities with Supermonodispersive Microspheres, *Phys. Rev. Lett.* **94**, 203905 (2005).
- [68] D. O’Brien, M. D. Settle, T. Karle, A. Michaeli, M. Salib, and T. F. Krauss, Coupled photonic crystal heterostructure nanocavities, *Opt. Express* **15**, 1228 (2007).
- [69] R. D. Meade, A. Devenyi, J. D. Joannopoulos, O. L. Alerhand, D. A. Smith, and K. Kash, Novel applications of photonic band gap materials: Low-loss bends and high q cavities, *J. Appl. Phys.* **75**, 4753 (1994).
- [70] P. R. Villeneuve, S. Fan, and J. D. Joannopoulos, Microcavities in photonic crystals: Mode symmetry, tunability, and coupling efficiency, *Phys. Rev. B* **54**, 7837 (1996).
- [71] D. F. Walls and G. J. Milburn, Effect of dissipation on quantum coherence, *Phys. Rev. A* **31**, 2403 (1985).
- [72] C. W. Gardiner and P. Zoller, *Quantum Noise: A Handbook of Markovian and non-Markovian Quantum Stochastic Methods with Applications to Quantum Optics*, 2nd ed. (Springer, Berlin, 2000).
- [73] Q. A. Turchette, C. J. Myatt, B. E. King, C. A. Sackett, D. Kielpinski, W. M. Itano, C. Monroe, and D. J. Wineland, Decoherence and decay of motional quantum states of a trapped atom coupled to engineered reservoirs, *Phys. Rev. A* **62**, 053807 (2000).
- [74] C. J. Myatt, B. E. King, Q. A. Turchette, C. A. Sackett, D. Kielpinski, W. M. Itano, C. Monroe, and D. J. Wineland, Decoherence of quantum superpositions through coupling to engineered reservoirs, *Nature (London)* **403**, 269 (2000).
- [75] Y.-x. Liu, i. m. c. K. Özdemir, A. Miranowicz, and N. Imoto, Kraus representation of a damped harmonic oscillator and its application, *Phys. Rev. A* **70**, 042308 (2004).
- [76] A. Megrant, C. Neill, R. Barends, B. Chiaro, Y. Chen, L. Feigl, J. Kelly, E. Lucero, M. Mariantoni, P. J. J. O’Malley, D. Sank, A. Vainsencher, J. Wenner, T. C. White, Y. Yin, J. Zhao, C. J. Palmstrøm, J. M. Martinis, and A. N. Cleland, Planar superconducting resonators with internal quality factors above one million, *Appl. Phys. Lett.* **100**, 113510 (2012).
- [77] <https://github.com/chenqmion/ScatteringCoefficients>.